Engineered Science
DOI: https://dx.doi.org/10.30919/es1399

Optimizing Hydrocarbon Recovery in Mature Fields: A Comparative Simulation Study of Infill Well Placement and Performance Using Integrated Reservoir Modeling Techniques

Emmanuel Emeka Okoro,[1, 2,*] Oscar I. O. Ogali,[1, 2,*] Samuel E. Sanni,[3, 4] Nubel Bariza,[1] Progress C. Mormah,[1] Ikechukwu Theophilus John[5] and Chukwuemeka Benjamin John[6]

Abstract

Infill drilling is a strategic method to improve hydrocarbon extraction and enhance field performance from mature oilfields, using strategies that involve an all-inclusive comprehension of reservoir dynamics. This study utilizes a meticulous reservoir-based simulation methodology for infill well positioning. Advanced modelling techniques were used to simulate three different scenarios involving two theoretical wells, Infill 1X and Infill 2X, to evaluate how strategically placed infill wells affect production rates. Other reservoir and well parameters considered include water-cut, average permeability at the perforation interval, reservoir pressure, and production rates. The Infill 1X well, located in a region with exceptionally high average permeability, is expected to generate a greater total amount of oil output over time. Nevertheless, the management of well production rates is essential for maintaining uninterrupted production and addressing concerns related to water-cut and gas-oil ratio (GOR) problems, as demonstrated by the performance of Infill 2X. The simulation results are further validated by applying the Darcy flow equation, which strengthens the conclusion that permeability plays a crucial role in hydrocarbon recovery. The study offers practical insights into the most effective positioning and operational control of infill wells, providing a strategy to rejuvenate mature oil fields and optimize extraction efficiency.

Keywords: Infill drilling; Mature fields; Reservoir-based simulation; Darcy flow equation; Well placement; Hydrocarbon recovery.
Received: 07 May 2024; Revised: 17 November 2024; Accepted: 02 December 2024.
Article type: Research article.

1. Introduction

The pursuit of energy self-sufficiency has compelled the oil and gas sector to optimize the extraction process from established reservoirs. Infill drilling, the process of drilling additional wells within existing oil and gas fields to exploit previously unexplored reserves, has emerged as a key aspect of reservoir management.[1] Nevertheless, the effectiveness of infill wells relies on a thorough comprehension of diverse geological and reservoir processes. Reservoirs are complicated geological formations that exhibit several characteristics, including porosity, permeability, and structural complexity.[2] Understanding these attributes is crucial as they govern the capacity of hydrocarbon storage and the movement within the reservoir, therefore establishing the optimal positions for infill wells.

The pressure regime of a reservoir governs the flow of fluids and has a significant impact on the performance of a well. Comprehensive knowledge of reservoir pressure systems is essential for preserving well integrity and maximizing hydrocarbon recovery rates through infill drilling.

[1] *Department of Petroleum and Gas Engineering, University of Port Harcourt, Rivers State, 500272, Nigeria*
[2] *Center of Petroleum Research and Training, University of Port Harcourt, Rivers State, 500272, Nigeria*
[3] *Department of Chemical Engineering, Covenant University, Ota, Ogun State, 112104, Nigeria*
[4] *Department of Chemical Engineering, Faculty of Engineering and Technology, Parul University, Gujarat, 391760, India*
[5] *Well Intervention Consultant, Shell Petroleum Development Company Limited, Port Harcourt, Rivers State, 500102, Nigeria*
[6] *OJT Trainer and Field Operations Coach, TotalEnergies, Port Harcourt, Rivers State, 500102, Nigeria*
**Email:* emeka.okoro@uniport.edu.ng (E. E. Okoro); oscar.ogali@uniport.edu.ng (O. I. O. Ogali)

Fluid dynamics governs the movement of oil, gas, and water within the reservoir. To accurately forecast the productivity of infill wells, it is crucial to have a deep understanding of the underlying dynamics.[3] This knowledge is essential to prevent undesirable outcomes such as the occurrence of water or gas coning, which can significantly hinder the overall performance of the well. Infill drilling outcomes are frequently predicted using sophisticated simulation models. These models utilize geology, pressure, and fluid data to predict reservoir performance and provide guidance for well placement.[4] Nevertheless, the precision of these forecasts relies on the caliber and comprehensiveness of the supplied data.

Examining historical data from production facilitates the comprehension of reservoir dynamics over the time frame of the data. This historical study can detect recurring trends and irregularities in reservoir performance, which can provide valuable insights for developing future infill drilling methods. Within the field of petroleum engineering, the process of developing a hydrocarbon reservoir is a crucial stage that involves strategically locating infill wells to maximize production.[5] The difficulty arises in the intricacy of underground habitats and the need to optimize the extraction of hydrocarbons while minimizing any negative effects on current well production. There are multiple perspectives, from which the background of a study on identifying the best areas for infill drilling can be examined. Well performance is significantly affected by reservoir heterogeneity, which encompasses the spatial arrangement of porosity, permeability, and hydrocarbon saturation.[6] Precisely charting these geological characteristics is crucial for comprehending the movement of hydrocarbons and devising a plan for positioning wells that focuses on untapped areas without negatively impacting the existing production zones.

An analysis of historical reservoir data offers valuable insights into production trends, variations in reservoir pressure, and the efficacy of past recovery methods. This information can assist in determining the optimal locations for infill drilling by identifying regions where output is decreasing or where there is untapped potential. Contemporary reservoir simulation techniques and advancements in seismic imaging enable a more thorough assessment of the reservoir.[7] These technologies facilitate the forecasting of fluid flow and detection of untapped reserves, assisting in the optimization of where to place more wells.

In addition to the technical concerns, it is crucial to evaluate the economic feasibility of infill drilling. This involves assessing the expenses related to drilling and completing the project, estimating the additional hydrocarbons that may be recovered, and considering the possibility of prolonging the lifespan of the oilfield. Operational factors, such as the availability of drilling equipment, potential risks while drilling, and the presence of pre-existing infrastructure, are also crucial in the decision-making process. Although there has been a significant advancement in reservoir engineering and management, there is still ambiguity in accurately predicting the behavior of intricate reservoirs. There is an ongoing requirement for research that combines several disciplines, like geophysics and data analytics, to improve infill drilling tactics.[8]

Cheng *et al*.[9] investigated techniques to improve the productivity of infill drilling in tight gas fields, with a specific focus on tight gas reservoirs. Although tight gas fields have poor production rates, they play a crucial role in the energy supply. Optimizing the placement of infill wells is essential for reviving fields with low permeabilities and narrow drainage areas. This optimization is necessary for increasing recovery and guaranteeing economic viability. The authors suggest a two-step approach: sequential inversion algorithm, which allows for quick history matching and relies on the correlation between permeability and porosity; and the successive selection strategy, which prioritizes the selection of infill well locations by taking into account the interference between existing and new infill wells, as well as among the infill wells themselves. By utilizing historical production data and employing dynamic reservoir modeling, this approach may effectively identify economically feasible infill wells and strategically determine their placement to optimize gas recovery and expedite field development.

The study conducted by Hutahaean *et al*.[10] aimed to optimize the placement of infill wells in mature oil fields, particularly in scenarios including the regeneration of brownfields, while taking into account geological uncertainty. The study discusses the difficulties of making strong decisions for placing infill wells in areas with unknown geology, particularly in brownfields where managing output decline is crucial. The objective is to optimize the extraction of oil while minimizing the costs associated with operations. The authors present a workflow that integrates multi-objective optimization, assisted history matching, Bayesian posterior inference, and optimization across several geological models. This comprehensive strategy seeks to offer strong and dependable decisions by precisely assessing geological uncertainty and economic hazards. The methodology is validated by conducting tests using a reservoir benchmark that is widely accepted and used in the industry. The results are contrasted with traditional uncertainty quantification methods, illustrating that the suggested workflow provides superior

estimation of uncertainties and decision resilience.

Chu *et al*.[11] examined the application of sophisticated machine learning methods to enhance the positioning of infill wells in the oil and gas sector. Their research focuses on the task of identifying the most effective locations for infill wells in reservoirs to maximize the extraction of hydrocarbons. Conventional approaches heavily depend on simulation, which can be both computationally expensive and time-consuming. The authors suggest a new method that utilizes a multi-modal convolutional neural network (CNN) to merge static and dynamic reservoir parameters in order to forecast the productivity of potential infill well sites. The objective of this method is to decrease the need for extensive simulation by offering a faster data-driven approach to assess well placement options. The predictions of the CNN model were verified by comparing them to the results obtained from classical simulations. The study findings indicate that the CNN model demonstrates a high accuracy in forecasting the productivity of infill well placements, exhibiting a significant concurrence with the simulation results while requiring fewer computational resources.

According to Malallah *et al*.,[12] infill well placement in heterogeneous reservoirs is difficult, especially when considering waterflooding, because of the intricate and extensive geological models. Their research presents a pragmatic and economical approach that utilizes wavelet transform to enhance the resolution of the geological model from smaller to larger scales, while maintaining important features. The purpose of this upscaling is to reduce the number of simulation runs and increase the amount of oil recovered by optimizing the position of infill wells. The methodology utilizes static Dykstra-Parson coefficients to evaluate reservoir heterogeneity and employs a streamlined simulation for computational efficiency. The validity of the approach is confirmed by testing it on three synthetic situations of two-dimensional inverted five-spot heterogeneous reservoir models. The findings validate that upscaling substantially decreases the necessary number of simulation iterations (ranging from 75% to 93%) and closely aligns with the oil recovery estimates of the initial fine-scale models. Their findings show that the practice of upscaling can significantly decrease processing resources and time requirements while still ensuring accuracy in identifying the most suitable well locations.

Gladchenko *et al*.[13] investigated the use of a data-driven method to improve the efficiency of infill drilling. They propose a modified capacitance-resistance model (CRM) that is further strengthened by including Kriging techniques. The research delineates the difficulties associated with positioning infill wells in oil fields, specifically in the presence of fluctuating field data and operational modifications. The authors suggest a new use of CRM combined with Kriging to improve the accuracy of predicting where new wells should be placed. The approach entails utilizing an adapted CRM that takes into consideration of well shut-ins and workovers by dynamically adjusting the model coefficients. Subsequently, this altered model is integrated with Kriging to spatially interpolate these coefficients, thereby optimizing judgments regarding the placement of wells. The research explores the optimization of CRM by utilizing past production data. The model is fine-tuned to incorporate operational changes and well interventions, hence, enhancing its ability to make accurate predictions. The technology enables the prediction of production patterns for newly drilled wells with little initial data, utilizing existing CRM coefficients and spatial interpolation by Kriging. The validity of the approach is confirmed through the use of both synthetic and real field data. Case studies provide evidence of the efficacy of the Kriging-boosted CRM in different situations, illustrating its ability to quickly assess and enhance infill drilling plans. The authors concluded that the integration of CRM with Kriging offers a reliable technique for determining the location of infill wells, which is capable of addressing the practical challenges posed by operational and data uncertainties. The technique is praised for its efficiency and scalability, making it capable of facilitating decision-making in reservoir management.

This study seeks to optimize the placement of infill wells in mature fields to increase hydrocarbon recovery. In order to accomplish this, one must master the intricacies of exact planning while also taking economic considerations and reservoir dynamics into account. This will be achieved through a comparative simulation analysis, which will provide a set of recommended practices for the placement and performance of infill wells. This study intends to utilize integrated reservoir modeling approaches to combine geology, geophysical, and production data to develop an accurate and detailed depiction of mature reservoirs. The research aims to produce a complete framework that reservoir engineers and field managers can use to improve decision-making processes. This novel methodology offers the potential to enhance the extraction of residual hydrocarbons, prolonging mature oil fields' operational lifespan. It also aims to improve the existing knowledge by providing practical insights into the complex relationship between reservoir parameters and infill drilling success.

To maximize production rates and field performance, it is necessary to determine where an infill well should be strategically positioned in a reservoir of interest to access

remaining reserves or zones with better productivity. This study is unique because it uses both static and dynamic reservoir models to predict where and how well infill wells will work. The study uses Petrel and PROSPER to create a static model of the reservoir well. Then, it uses Eclipse to model and simulate the well under different situations. Infill well performance can be investigated in depth using this method by examining the effects of variables including water cut, average permeability around the perforation interval, pressure, and production rate. To further highlight the impact of permeability on recovery rates, the study offers a strong methodological framework for optimizing the placement of infill wells in complex reservoir environments. It also includes validation of the simulation results using the Darcy flow equation, which is unique.

2. Methodology

To achieve maximum hydrocarbon recovery, it is crucial to have a thorough understanding of how the distribution of remaining hydrocarbons in the reservoir changes over time. This knowledge is essential for determining the best locations to drill additional wells.[14] The optimal production plan is placing the infill well in regions with the greatest concentration of hydrocarbons, known as "sweet spots". The use of net oil map plots is crucial in determining the thickness and distribution of remaining hydrocarbon saturations. This information is essential for strategically locating infill wells. To achieve the goals of this study, the approach is divided into two separate phases: first, the creation of a stationary geological and geophysical model, and second, the establishment of a dynamic model. The utilization of this dynamic model is essential for accurately determining the initial volume of hydrocarbons in a reservoir and for assessing the impact of strategic infill well placement on reservoir performance. This is achieved through the implementation of the net oil map approach.

2.1 Data source

For this project, an extensive dataset comprising geological data, field data, reservoir characteristics, and fluid properties was utilized. The data were sourced from actual spreadsheet files and well log records, from a field, dubbed Field "X". These comprehensive datasets underpin the analysis and modeling efforts undertaken in the study.

The data used in this study was obtained from many important sources, such as well logs, seismic data, core samples, and production data from the reservoir, Field "X". The data sources were carefully chosen to appropriately reflect the geology and reservoir characteristics relevant to the study area. Seismic interpretation was conducted to establish the structural framework of the reservoir by identifying important elements such as faults, folds, and horizons. The seismic data underwent depth conversion and were incorporated into the three-dimensional (3D) structural model. The well log data, which include gamma-ray, resistivity, density and neutron logs, were employed to identify lithology and estimate porosity and permeability. The logs were adjusted for environmental factors, and the porosity and permeability values obtained from the logs were compared with core data, if it was accessible, to ensure accuracy. The log interpretations and petrophysical models were refined by calibrating them with core data, which included measurements of porosity, permeability, and fluid saturation. The core data served as an accurate reference for the geological attributes of the reservoir. The dynamic reservoir model was calibrated and validated using historical production data from the Field. This stage ensured that the model's predictions were following the observed performance in the field. The field operator conducted seismic surveys, retrieved well logs, and collected core samples to gather geological data. The data collection encompassed lithology logs, measurements of porosity and permeability, as well as structural mapping. The site data were obtained via drilling reports and field development plans, which included information on well locations, trajectories, and completion details.

Quality control (QC) was a crucial component of the data processing workflow to guarantee the dependability and precision of the geological model and subsequent property modeling. The input data underwent thorough validation checks, which included ensuring consistency between well logs, core data, and seismic interpretations. Any inconsistencies were resolved by either recalibrating or excluding unreliable data points. The structural model underwent a review to ensure its geometric coherence, with special emphasis on the alignment of faults and horizons. The grid underwent a thorough examination to identify any abnormalities, and any problem found was addressed by making improvements to the grid. During the process of property modeling, variograms were examined to verify that the spatial arrangement of attributes, such as porosity, permeability, and facies, aligned with geological predictions. Several instances of property models were created to account for uncertainty, and these were verified using core data. The initialized static and dynamic models were compared to establish coherence in volumetrics and fluid distributions. The dynamic model was calibrated using production history matching, which further confirmed the accuracy of the model's predictions.

2.2 3D Geologic modeling

A detailed 3D static model was created for the reservoir in Field "X" to aid in evaluating the volume of hydrocarbons present and to assist in dynamic simulations for projecting the performance of the field. This model combines information from seismic surveys, thorough geological maps, and rigorous petrophysical investigations to construct a strong and accurate depiction of the underground layers. The construction of the static model involves a series of important phases, all designed to improve the accuracy and utility of the model for future dynamic simulations and decision-making.[15]

The well log data from wells X1, X2, and X3 were converted into a digital format and standardized to a uniform format. The core data were aligned with the depth of the well logs. The seismic data underwent processing to enhance vertical resolution. The consistency of log data across wells was assessed by analyzing cross-plots and histograms. To develop the cross-plots and histogram, well logging files, usually in Log ASCII Standard (LAS) format, are extracted to create log data cross-plots and histograms. Petrel, Techlog, Pandas, and Matplotlib import these files. Histograms arrange data by log parameter (*e.g.*, gamma ray, porosity, and resistivity) into bins that indicate parameter values and intervals.

The frequency of data points in each bin was calculated and plotted to visualize the distribution. Cross-plots were used to compare two log characteristics (*e.g.*, porosity vs. density) on a scatter plot. The process was repeated for numerous wells, frequently using various colors or symbols to distinguish data. This graphically compares trends and variances. Customizing histograms and cross-plots with scale, axis labels, and statistical overlays makes them great consistency analysis tools. Outliers were detected and subsequently addressed or eliminated based on geological comprehension. Seismic-to-well ties were conducted to guarantee precise conversion of time to depth.

Wells were linked together by identifying and comparing important stratigraphic indicators. The selection of tops was based on the characteristics of the well logs and cross-validated across different wells to ensure consistency. Isochore maps were created to verify the accuracy of the structural structure. Well log and seismic data are used to create an isochore map, which shows the true vertical thickness of a geological formation or reservoir unit. Gamma ray and resistivity well logs identify the formation tops and bottoms. To adjust the directional wells, true vertical thickness (TVT) is computed for each well by subtracting the top depth from the bottom. Time-thickness intervals are translated to depth using a velocity model using seismic data. Mapping software like Petrel, ArcGIS, or Surfer plots these estimated thickness values at well or seismic data sites. The data points are interpolated using kriging or inverse distance weighting to build a continuous map of thickness variations over the area of interest.

The isochore map is modified with geological inputs to correlate with structural trends or depositional characteristics and checked against additional data if available. The finished map helps exploration and development planners understand reservoir geometry and volumetrics. The selection of tops was meticulously made by utilizing a blend of seismic and well log data. The correctness of well tops was verified by comparing them with seismic horizons and confirming that they were aligned with depth-converted seismic data. Any discrepancies were resolved by improving the seismic interpretation or modifying the well tops using well log data. Seismic fault sticks were used to accomplish fault modeling. The fault model underwent a quality check to ensure its compatibility with well data and seismic interpretations. The horizons were subsequently modeled, taking into account both the well tops and seismic choices.

The facies were initially modeled using sequential indicator simulation, using constraints from well data and guidance from an understanding of depositional processes. The petrophysical parameters were modeled inside each facies using sequential Gaussian simulation, which ensured that the well data were respected and that the spatial distribution was adequate. The initial model was verified using well data and based on basic geological understanding. The discrepancies were resolved by continuously improving the structural framework and property allocations. This method was iterated until sufficient correspondence with all accessible data was attained.

The verified seismic data were utilized to construct the structure of the reservoir. This involved generating faults and horizons, which were then incorporated into the 3D grid. The structural model underwent multiple iterations to ensure its alignment with well tops and seismic interpretations. The grid was populated with petrophysical parameters, such as porosity and permeability, using well-log data. Facies modeling was performed by utilizing well logs and seismic features to guarantee a geologically accurate distribution of properties. The property models underwent quality control checks, which included variogram analysis, to verify their spatial coherence with the geological context.

The ultimate objective of these endeavors was to acquire a profound comprehension of the reservoir's attributes, which is crucial for optimizing recovery strategies and improving overall field development.

2.3 Reservoir description

The well log study undertaken in Field "X" indicates notable disparities in reservoir thickness, ranging from 252 ft in the Well X1 to 414 ft in the Well X3. The reservoir's geological structure is classified as a four-way rollover anticline with a north-south axis orientation, which is a typical structural trap seen in hydrocarbon basins. The reservoir's depositional environment is generally understood as shoreface and distributary channel systems based on the unique well-log signatures detected.[16,17] These habitats are usually identified by the accumulation of "clean", well-arranged sediments, as confirmed by the log data showing mostly homogeneous and consolidated sand formations in the reservoir. The reservoir contains an oil column with an average height of 87 ft, overlaying an aquifer with an average thickness of 170 ft. With an estimated average porosity of 33% and average permeability of 1,434 mD, this reservoir has the potential for significant fluid flow and recovery of hydrocarbons. Figs. 1 and 2 provide additional in-depth geological and structural information through the depth structure map and the structural correlation of the wells in Field "X", respectively. These pictures depict the spatial connections and uninterrupted nature of the reservoir formations, facilitating a thorough comprehension of the reservoir's shape and areas with a potential for productivity.

2.4 Structural modeling

The structural model is the fundamental framework for the geological modeling process, serving as the basis for developing all other reservoir features. The process consists of three essential steps: fault modeling, pillar gridding, and vertical layering.[18] Each stage played a vital role in guaranteeing a precise and comprehensive three-dimensional structure.

2.4.1 Modeling of faults

Fault modeling is an essential process for accurately representing the intricate geological formations in the reservoir. While Field "X" did not exhibit any faults, our usual procedure for fault modeling includes the following steps: importing fault sticks from seismic interpretation, doing quality checks on fault intersections and truncations, generating fault surfaces, and defining fault linkages and truncations.

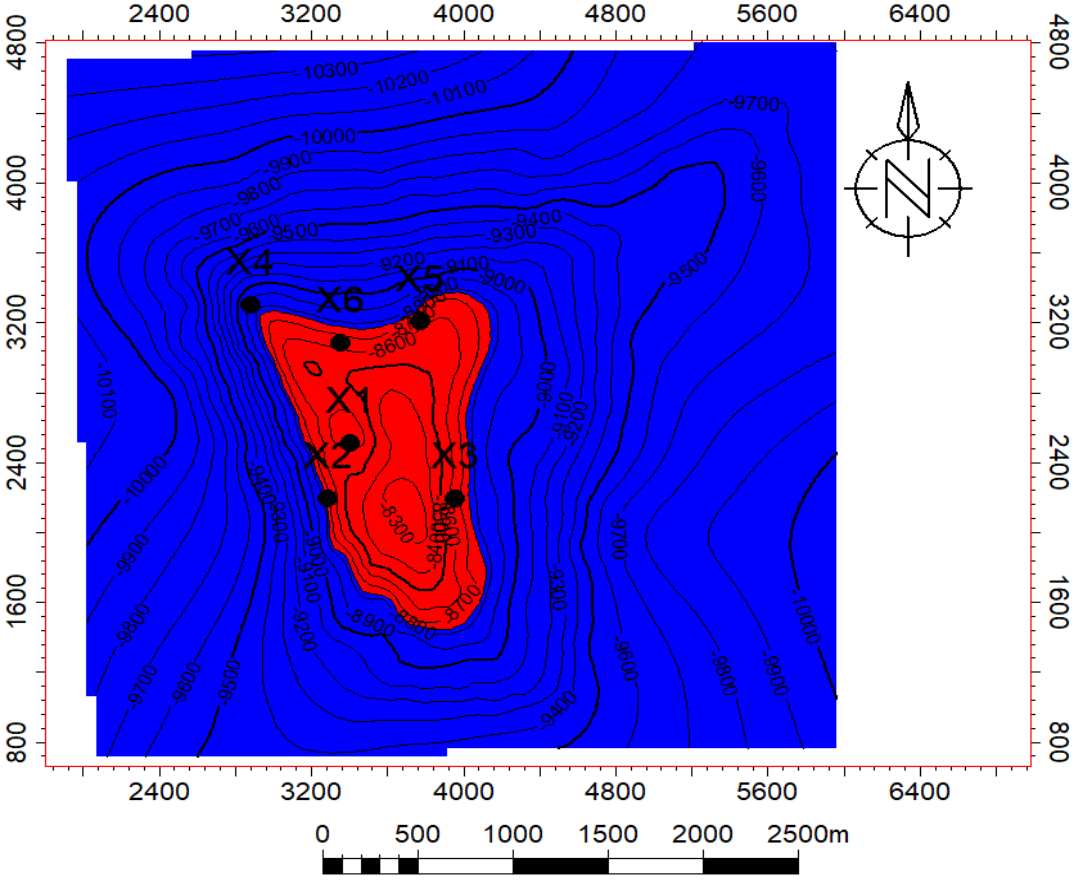

Fig. 1: Field "X" reservoir depth structure map. The map shows the four-way rollover anticline structure with oil and underlying aquifer. X- and y-axis parameters represent spatial distances in meters over a region. These axes display traditional Cartesian coordinates for the map's horizontal extents. The bottom grid (labeled "0, 500, 1000, 1500, 2000, and 2500 m") shows that the x- and y-axes are in meters (culled from an unpublished report).

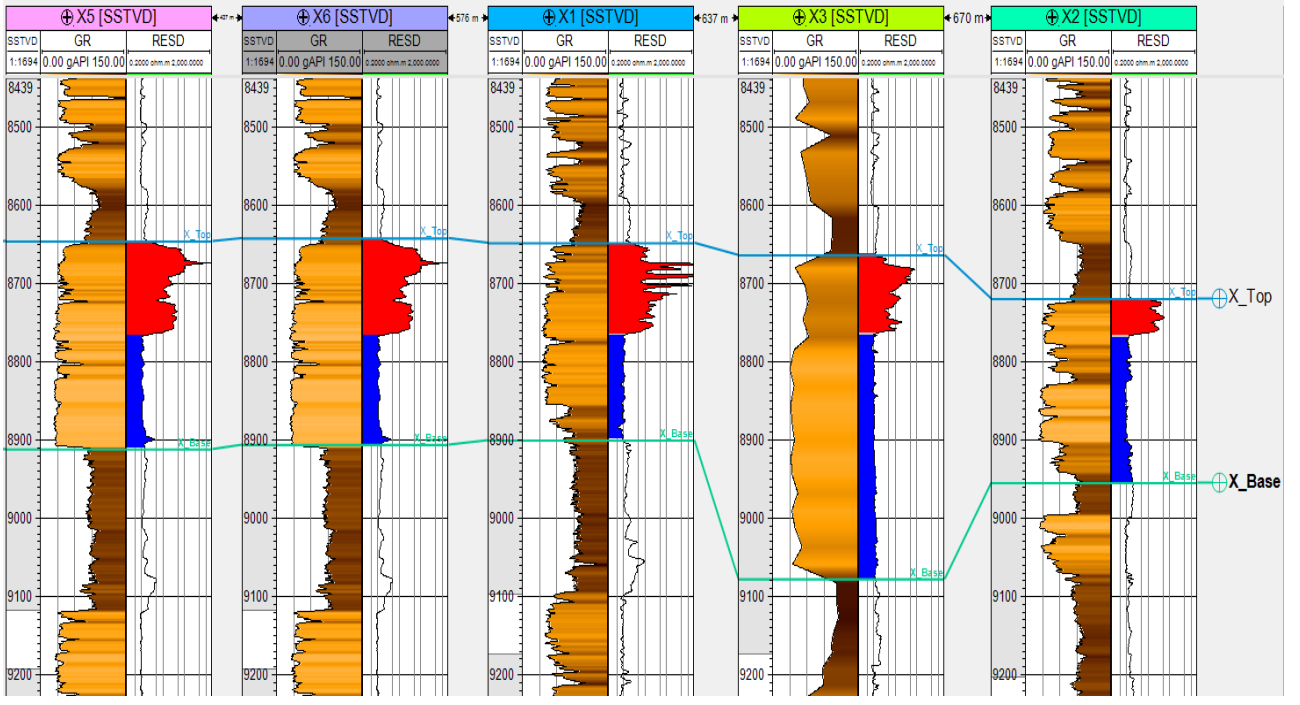

Fig. 2: Well correlation and fluid distribution for Field "X". This shows two well logs (Gamma Ray, GR, and Resistivity, RESD) for five wells in Field "X", highlighting the top and base lines, and the lithology variations and fluid types between wells (culled from an unpublished report).

2.4.2 Pillar gridding refers to the process of creating a grid system using pillars

Pillar gridding refers to the procedure of constructing a three-dimensional grid that establishes the spatial structure of the reservoir. The initial stage of pillar gridding entails creating a skeletal framework composed of top, middle, and base skeletal grids. This framework establishes the foundational grid structure that will be further developed in the following stages. A grid lattice with a resolution of 50 m × 50 m was chosen to precisely depict the structural intricacies of Field "X". The grid density was selected to strike a balance between the requirement for intricate information and computing performance. The pillar grid underwent thorough quality control, which involved conducting inspections for grid crossing and discrepancies in grid spacing. This guaranteed that the grid precisely depicted the geological characteristics without introducing any artifacts that could distort the reservoir model.

2.4.3 Vertical stratification

Vertical layering is crucial for precisely recording the geological characteristics and vertical resolution of the reservoir. The process of vertical layering was determined by seismic horizons and geological zonation. The primary reservoir layers were defined using key stratigraphic surfaces discovered in the seismic data, while vertical heterogeneity was further characterized using well-log data. The vertical resolution of the grid was established by dividing the highest recorded isochore (thickness) by a uniform cell thickness of 2 feet. This method guaranteed that the grid could accurately represent small-scale vertical differences in the reservoir properties, which is crucial for precise property modeling. The ultimate vertical cell resolution was determined by combining the seismic and geological data, guaranteeing that the layering precisely reflected the intricate stratigraphy of the reservoir.

Subsequently, pillar gridding is utilized to construct a well-organized 3D grid that covers the complete geological volume of the reservoir. This gridding technique entails establishing vertical pillars that are precisely aligned with geological features such as faults and horizons, ensuring that the grid represents the intricate geometries of the subsurface structures. The construction of the corner-point 3D grid of Field "X" involved the use of pillar gridding. This method includes the production of a skeleton framework, which consists of three main components: Top, Mid, and Base skeleton grid. To accurately represent the intricate structure and subtle variations of each layer in the reservoir, each grid cell with a size of 50 m by 50 m was used. Quality control tests were implemented to ensure the integrity and accuracy of the pillar grinding process. These checks specifically involved confirming that there were no crossing pillars, as this might lead to problems in the grid geometry.

The model's vertical layering component entails splitting the geological region into distinct horizontal strata. The

stratification is established using seismic horizon data, which offers comprehensive insights into the layering and uninterrupted distribution of several stratigraphic strata inside the reservoir.[19] The grid's layers are assigned attributes based on geology and petrophysical data, which improves the model's capacity to forecast reservoir behavior in different production scenarios.

A geological stratum or horizon can be represented by a plane equation in 3-D space, as shown in Eq. 1. Equation of a plane delineates stratigraphic surfaces or basic structural strata. For inclined strata, the parameters a, b, and c denote the dip and strike of the plane, whereas d vertically displaces it. This equation is essential in structural models for depicting continuous layers or horizons throughout a field.

$$ax + by + cz + d = 0 \quad (1)$$

where a, b, and c are the directional cosines representing the orientation of the plane; x, y, z are the coordinates of any point on the plane, and d is a constant that adjusts the plane's position in space. For a specific stratum, dip refers to the highest angle of inclination, whereas strike denotes the direction perpendicular to the dip. These are crucial for the fabrication of three-dimensional representations of sloped layers.

For calculations of dip and strike, given a vector (Eq. 2), the dip angle (θ) is calculated using Eq. 3.

$$\vec{n} = (a, b, c) \quad (2)$$

$$\theta = arctan\left(\frac{\sqrt{a^2+b^2}}{c}\right) \quad (3)$$

Strike direction: The strike can be derived from components a and b, which denote the orientation on the horizontal plane. Dip and strike calculations provide the precise orientation of geological layers, essential for subsurface interpretations and well planning.

2.5 Reservoir gridding quality control

The structural integrity and accuracy of Field X's grid underwent a thorough validation process using a complete QC procedure. The results of this process, together with the structural visualizations, are provided in Fig. 3. The upper, middle, and lower skeletal grids were thoroughly examined for any discrepancies. This stage is crucial in guaranteeing that the fundamental layers of the grid precisely depict the geological structure of the reservoir. The pillars were examined by analyzing their I (inline) and J (crossline) intersections, to identify any geometric abnormalities or instances where pillars intersected, which might potentially undermine the structural integrity of the grid.[20] Seismic horizons were overlaid with gridlines to visually verify their alignment and uniformity. This aids in confirming the precise alignment of the grid with the geological horizons and features that have been found through seismic data. A volumetric property model was created using geometric modeling techniques.

This model underwent a thorough examination to identify any negative volumes, which can indicate potential issues in the grid, such as overlapping cells or inaccurately described geometries. To further improve the quality control process, property models were created that specifically target cell angle and cell inside out.[21] These models help to detect any cells that may have been reversed during the gridding process or cells with angles that deviate greatly from the expected standard, both of which can affect the quality of the simulation. This comprehensive quality control approach ensures that the 3D grid of Field X complies with the necessary criteria for structural and geometrical accuracy, establishing a strong basis for reliable dynamic modeling and reservoir management strategies.

2.5.1 Reservoir property modeling

Property modeling is the process of filling the cells of a 3D geological grid with different reservoir properties, which can be classified as either discrete (such as facies) or continuous (such as porosity, permeability, and water saturation), after confirming the accuracy of the reservoir's geometric framework. The distribution of continuous features in this process is usually limited by the facies model, which is based on a well-developed conceptual geological model.[22]

The development of this conceptual model entails examining core samples obtained from reservoir sequences to comprehend the depositional settings and sediment dynamics. By including interpreted facies distributions obtained from 3D seismic data, it is possible to accurately define the spatial variations within the reservoir. Utilizing a comprehensive set of high-resolution wireline logs enhances the geological model by incorporating precise subsurface lithological data.

The Field "X" wells were analyzed by generating facies logs, which involved identifying sand, silt, and shale facies using Vshale (V_{sh}) curves with defined thresholds: sand was classified as values below 0.55, silt was classified as values between 0.55 and 0.65, and shale was classified as values above 0.65. The thresholds were determined using a cross-plot analysis of Vshale and porosity, ensuring a statistically reliable basis for distinguishing facies. Afterward, the facies logs were converted to average values and entered into the grid cells that were aligned with the trajectory of the wellbore.

The horizontal variogram analysis was performed to determine the primary and secondary distances at which facies are distributed across the reservoir. This analysis helps in the

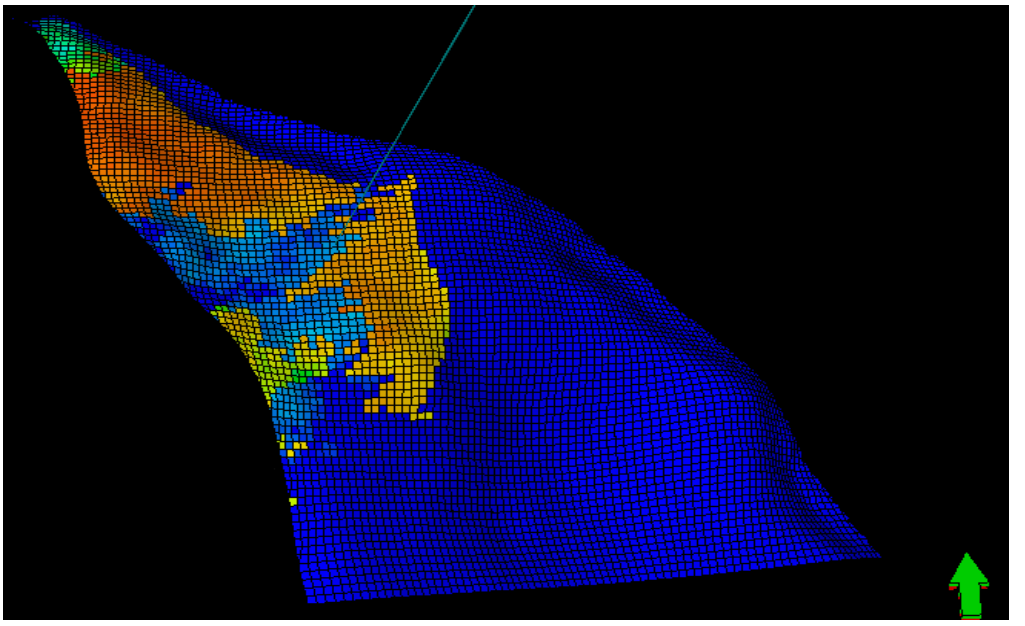

Fig. 3: 3D model of the reservoir with fluid contact. This provides a spatial view of the reservoir with the fluids and fluid contacts: blue for water and yellow/orange for hydrocarbons. (culled from an unpublished report).

spatial modeling of the continuity and heterogeneity of facies. The analysis of facies modeling involved studying the vertical distribution of facies inside the Field X model, evaluating the variance in the thickness of facies bodies, and creating a discrete variogram to characterize the spatial distribution of facies. The sequential indicator simulation (SIS) algorithm was employed to interpolate facies over the reservoir. This technique leverages binary indicators to stochastically produce facies distributions.

The integration of vertical proportion curves was used to regulate the vertical arrangement of facies among wells, ensuring that the facies model precisely represents the stratigraphic variations found in the core and log data. The resulting facies model was subjected to thorough quality control by comparing the facies logs generated at different well locations with the modeled facies.[23] This was done to ensure that the facies representation across the reservoir is consistent and accurate. This holistic approach to property modeling not only strengthens the reservoir model with crucial geological insights but also improves the predicted accuracy and reliability of reservoir simulations and development methods.

2.5.2 Net-to-Gross, porosity, permeability, and water saturation modeling

The Net-to-Gross (NTG) ratio, computed from $1 - V_{sh}$ (where V_{sh} represents the volume of shale), was extended into three dimensions from well data where NTG values had been upscaled. This extrapolation employed sequential Gaussian simulation (SGS) methodologies, resulting in a comprehensive cellular model that assigns precise NTG values to each cell. This method facilitates a representative description of the reservoir pore volume distribution and reservoir quality, which are used for storing and flowing hydrocarbons, respectively.[24]

For porosity, the upscaled curves representing total porosity, ϕ_t, and effective porosity, ϕ_e, were spatially modeled across the grid using SGS. The technique was improved by linking the distribution of porosity to different rock types, which allowed for the inclusion of geological variations in the porosity model and improved the model's ability to make accurate predictions. The permeability model was formulated using a porosity-transform relationship, which was mathematically generated from an empirical association discovered in the core data. This method accurately converts porosity data into estimations of permeability, establishing a crucial connection between observable rock attributes and fluid flow characteristics.

The water saturation within the reservoir was simulated using a saturation-height function, which was derived from a thorough review of petrophysical evaluation criteria. This function facilitates the dispersion of water saturation throughout the reservoir by establishing a correlation between saturation levels and the distance above the free water level, thus providing a saturation profile that follows the saturation profile of Field "X".[25] The geographical distribution of these reservoir features was determined using an exponential variogram model. The model was created from horizontal variogram analysis and had horizontal ranges of 2,500 to 3,500 m. Additionally, a vertical range of 10 ft was included. This

variogram setup enables the accurate representation of the relationships between properties at different distances, both horizontally and vertically, inside the reservoir.

Figs. S1-S6 (see supporting information file) present visual representations that demonstrate the distribution and variability of reservoir parameters such as NTG, porosity, permeability, and water saturation. These visual representations provide useful insights into the spatial variability of reservoir properties, which are crucial for informed reservoir management and development planning.

The pressure-volume-temperature (PVT) samples collected from the evaluated wells, X-1 and X-2, are crucial for simulating the characteristics of the reservoir fluids. The samples were obtained at different depths in order to encompass the whole spectrum of conditions present in the reservoir. Their representativeness was confirmed through a series of stringent laboratory tests, which included constant mass expansion, differential liberation, and viscosity measurements conducted under separator settings. In order to guarantee the dependability and precision of the laboratory fluid data, additional validations were carried out using relative volume, viscosity tests, and Y-function studies, which evaluate the behavior of the fluid under simulated reservoir conditions.

The core experiments yield supplementary data, including relative permeabilities, capillary pressure measurements, and rock compaction investigations, which offer precise information about the presence, saturation, and distribution of fluids within Field X. These tests are essential for comprehending the dynamic interactions between the fluids in the reservoir and the rock matrix, which allows for a thorough assessment of the petrophysical parameters of the reservoir.[26] Petrel RE software enables the seamless incorporation of the fluid model and the special core analysis laboratories (SCAL) data into the geological grid structure. This advanced reservoir engineering tool enables precise simulation of the initial condition of the reservoir. The oil-water contact (OWC) and the initial reservoir pressure, both of which are crucial factors, are carefully simulated in the reservoir model to guarantee its stability and precision. These parameters are referenced to a specific datum for accuracy. This integration not only improves the forecast accuracy of the reservoir simulations, but also facilitates optimized reservoir management and development methods.

Several fluid characteristics of Field "X", which are related to the crude oil, include initial oil-in-place and initial oil formation volume factor. These parameters are crucial for determining the existing reserves and recoverable reserves from Field "X", as well as identifying apposite development and production strategies for Field "X".[27] Initial oil in place refers to the aggregate quantity of crude oil present in the reservoir of interest prior to production and development. Field "X" has an initial oil in place of 91.78 million barrels of oil (91.78 MMBO). The initial oil formation volume factor, B_{oi}, refers to the volume at the surface (or under surface conditions) required to replace one barrel of oil in the reservoir (or under reservoir conditions), or the degree of oil expansion between the reservoir conditions and surface conditions. The B_{oi} of Field "X" is 1.132 RB/STB (RB is for reservoir barrel; STB is for stock tank barrel), meaning that the stock tank oil originally in place (STOOIP), which is the initial crude oil at surface conditions, is 81.08 MMSTBO.

2.6 Property modeling

The property modeling approach entailed filling the geological grid cells with both discrete (facies) and continuous (porosity, permeability, water saturation) qualities. The process was executed in a sequential fashion to guarantee geological coherence.

2.6.1 Facies modeling with discrete property

The process of facies modeling was carried out by following these steps:

Facies logs were created for Field X wells by determining sand, silt, and shale facies using Vshale curves with cut-off values of 0.55, 0.55-0.65, and 0.65, respectively. The facies logs that were produced were upscaled in order to assign average values to the cells along the wellbore. An examination of the horizontal variogram was performed to ascertain the primary and secondary distances over which facies are distributed. The SIS approach was used to interpolate the facies. Facies distribution between wells over the area of interest was achieved by including vertical proportion curves. The resulting facies model underwent a quality check by comparing the facies logs obtained at various well locations with the modeled facies.

2.6.2 Continuous property modeling

The continuous qualities of porosity, permeability, and water saturation were represented in the following manner:

Porosity Modeling: Upscaled porosity curves (PhiT, PhiE) were simulated between cells using sequential gaussian simulation. The porosity model was adjusted to the facies model in order to maintain geological coherence.

Permeability Modeling: A permeability model was created by applying a mathematical transformation to the porosity data. The transformation was created analytically based on actual relationships discovered from core data. The resulting

permeability model underwent quality assurance by comparing it to well data and core measurements.

Modeling of water saturation: The distribution of water saturation was determined using a saturation height function derived from petrophysical evaluation criteria. The model accurately incorporated the initial water saturation levels at the well locations and maintained consistency with the structural structure.

NTG Modeling: The NTG value, obtained from 1-Vsh, was estimated in three dimensions using upscaled NTG data from wells. NTG values were assigned to each cell using sequential Gaussian simulation.

The property distribution utilized an exponential variogram with ranges of 2,500 m and 3,500 m, as determined through the horizontal variogram analysis, along with a vertical range of 10 feet for all continuous properties.

2.7 Data quality control and quality assurance

In implementing data quality control and quality assurance, the collation of different datasets required for this study was systematic and integrated. Several datasets were required and as such, adoption of quality control and quality assurance procedures were applied to ensure data consistency across these datasets. Reservoir rock properties were largely collected from seismic surveys, well logs, and core analyses. Besides the seismic surveys, data collected from wells (well logs and core analysis data) means that there was limited information on other parts of the reservoir. This is typically the case for most reservoir characterization and simulation processes. Geostatistical techniques like kriging, SIS, and SGS were therefore used to spatially interpolate reservoir rock properties, and their results were validated using datasets obtained at the wells. This is the standard practice in reservoir characterization and simulation workflows. Prior to applying geostatistical techniques, the datasets obtained (reservoir rock properties data) were cross-referenced from multiple reliable sources (well logs, core data) for Field "X", and quality checks were conducted to detect and eliminate erroneous measurements.

Historical production data from wells were obtained from Field "X". The production rates obtained from simulations were validated using the observed production rates from Field "X", to verify their consistency and ensure that inferences made from the study were applicable to the actual Field "X". The simulation grid was also selected, such that it adequately captures the reservoir heterogeneity of the Field "X" without being unnecessarily complex to require huge computation resources. History-matching between simulation results and production data was carried out to ensure that the simulation model accurately predicts Field X's behavior and that discrepancies are minimized by achieving a satisfactory history match.

3. Dynamic simulation of field "X"

A 3D-dynamic simulation of Field "X" was used to carefully predict the strategic positioning of infill wells to improve reservoir recovery. The dynamic model was created by combining Field X's geology and petrophysical data with dynamic engineering datasets.[28] These datasets contain fluid characterization data (PVT) that provide detailed information about the distinct properties of the reservoir fluids, the distribution and limits of fluid saturation, and rock-fluid interaction data obtained from Special Core Analysis Laboratories (SCAL). Furthermore, the model integrates pressure equilibration data, which is crucial for precisely initializing the pressure of the reservoir model, as well as equilibrating the model. Once the model was initialized, it was used to conduct prognostic simulation runs to maximize hydrocarbon recovery by strategically placing wells.

3.1 Fluid modeling (PVT)

The PVT data collected for the Field X is presented in Table 1. Field X has an initial reservoir pressure of 2,016 psia and a bubble-point pressure of 1,850 psia. The bubble-point pressure is the pressure at which gas bubbles first appear in the oil.[29] This shows that Field X is an undersaturated oil reservoir. The initial oil formation volume factor (B_{oi}) and initial oil viscosity (μ_{oi}) are 1.132 RB/STB and 7.02 cP respectively. The oil viscosity impacts the oil flow in the reservoir. The higher the oil viscosity, the lower the oil production rate in the reservoir.[29] The initial solution gas-oil ratio (R_{si}), which is the amount of gas dissolved in the oil initially, is 256 scf/STB. The oil's API gravity is 23.7 ^{o}API, making it a medium crude based on its density. The gas gravity in Field X is 0.618. These qualities are crucial in determining the characteristics of the reservoir fluid and are vital for reservoir simulation, development planning, and predicting future performance.

3.2 Rock and fluid property modeling

The relative permeability curves were calibrated using recognized sand facies due to the lack of core analysis data for Field X. The initial water saturation (S_{wi}) for each facies in the model was determined based on different rock types identified from the water saturation versus height above free water level (HAFWL) plot. The capillary pressures for each facies type were estimated by calculating the difference in density between oil and water at a specific reference height (h) above the free water level. The calculated capillary pressure was then

Table 1: PVT data for X-field reservoir fluid.

Initial reservoir pressure (P_i) (psia)	Bubble-point pressure (P_b) (psia)	Formation Volume factor (B_o) (rb/STB)	Viscosity (μ_o) (cP)	Solution gas (R_{si}) (scf/STB)	API°	Gas gravity (γ_g)
2,016	1,850	1.132	7.02	256	23.7	0.618

used to determine and improve the scaling of initial fluid saturations in each grid block of the model. Iterative modifications were made to the initial water saturation (S_{wi}) values to create a uniform and accurate static volume match across the reservoir model.[30]

Fig. 4 displays the refined relative-permeability curve for the dominant sand facies in the reservoir. This curve is crucial for simulating fluid flow through the porous medium and improving estimates of reservoir performance. As anticipated, the water relative permeability (k_{rw}) rises in proportion to the water saturation. At low water saturations, the k_{rw} value is essentially 0, suggesting that water remains stationary until it reaches a specific saturation threshold, called the critical water saturation (S_{wcr}). The oil relative permeability (k_{ro}) decreases as the water saturation increases, indicating that as the reservoir becomes more saturated with water, the oil's capacity to flow through the porous medium declines.

The result conforms with the accepted petrophysical principles, which state that in a two-phase system consisting of oil and water, the flow capacity of one fluid decreases as the saturation of the other fluid increases.[31] This is because these two fluids compete for flow paths in the porous medium. Upon comparing these findings with existing scholarly works, it is evident that the patterns seen in this study are consistent with traditional relative permeability models for sandstone reservoirs. Corey's correlations provide a foundation for understanding the behavior of relative permeability, which would exhibit similar patterns as depicted in the graph. According to Corey's model, k_{rw} increases as the water saturation (S_w) increases, following a power law relationship. On the other hand, k_{ro} generally decreases as a power law function of oil saturation (S_o). In a system without gas, the oil saturation is complementary to the water saturation.

3.3 Field X reservoir initialization and prediction models

The reservoir was initialized by methodically including essential petrophysical data, such as porosity, permeability, and fluid saturations, together with crucial geological information, which includes the structural grid, geological contacts, and facies distribution of Field X. The integration of these extensive datasets, in addition to previously established PVT and SCAL (Special Core Analysis Laboratories) data, played a crucial role in determining the initial volume of hydrocarbons in place (IHCIP). The model was carefully developed to ensure the initial conditions closely matched the initial conditions of the actual reservoir, including the fluid saturations and pressure distributions.[32] Three wells were drilled into the actual reservoir. However, only one of them, called X1, was finished. A drill stem test (DST) was conducted on this well, yielding significant dynamic data that indicated the reservoir's ability to generate fluids.

The knowledge obtained from the DST was utilized to create a thorough well model using PROSPER software. In this model, we built the inflow performance relationship (IPR) and vertical lift performance (VLP) tube curves. These graphs depict the capacity of the well to produce and the correlation between the rate of flow and the decrease in pressure along the tubing, respectively. Afterward, the calculated IPR/VLP curves were incorporated into the prediction models. This interface enables the Eclipse reservoir simulator to quickly access pertinent data for interpolation or extrapolation purposes during the prediction runs, hence improving the efficiency and accuracy of production estimates.[33]

Furthermore, the reservoir model's projected scenarios were subjected to particular operational limitations, which were set as predetermined limits. These constraints are in place to ensure the simulation scenarios are within realistic and attainable operational parameters, thereby reflecting the practical limitations faced during real reservoir management. The development scenarios considered are:

1. Case 1: Produce with existing well 1X.
2. Case 2: Produce with an Infill well (Infill-1X) targeting the sweet spot.
3. Case 3: Produce with an Infill well (Infill-2X) away from the aquifer.

3.4 Well model/lift curves export

The PROSPER software, which is part of the integrated production modeling (IPM) suite, was used to simulate the wellbore configuration of well X1. The simulation was adjusted to match the results of the DST. The Darcy IPR model, which is based on Darcy's law, was used for the IPR component of the X1 well model. This model describes the flow of fluids through porous surfaces. The most effective

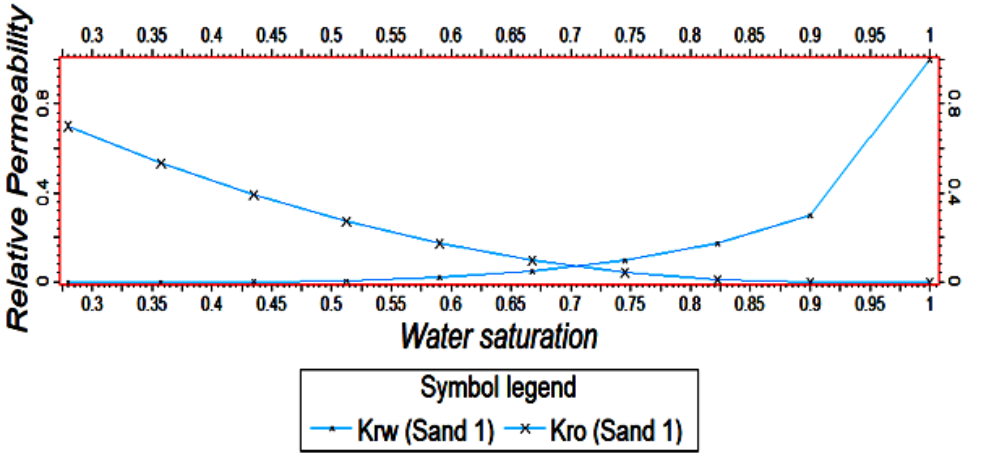

Fig. 4: Relative-permeability plot for Sand 1 in Field "X". This shows that Sand 1 is strongly water-wet with a connate water saturation of about 0.44.

Table 2: X1 DST IPR/VLP matching results.

	Tubing head pressure (psia)	Tubing head temperature (°F)	Watercut	Liquid rate (STB/day)	Gauge depth (ft)	Gauge pressure (psi)	Reservoir pressure (psi)	GOR (scf/STB)
X1 DST (Input data)	590	92.5	0	675	4,541	1,967	2,016	256
X1 DST (Matched data)	590	92.5	0	680	4,541	1,967	2,008	256

approach for achieving the VLP matching process was utilizing the approaches offered by Petroleum Experts 2. The DST findings were consistent with the stock tank oil rate of 676 STB/day, as calculated by the PVT analysis carried out on fluid samples obtained from the separator. This confirmed the precision of the PROSPER model in accurately representing the production capacity of the well.

The data obtained from the initial simulation and the final matching results of the well X1 PROSPER model are consolidated in Table 2. Furthermore, Fig. 5 visually demonstrates the link between the IPR and VLP. The model was enhanced to include the specific perforation intervals planned for the potential infill wells.[34] A subsequent re-matching operation was carried out without requiring any substantial modifications to the previously matched data, demonstrating a strong and consistent model configuration.

Table 2 displays the input and matched data for the DST conducted on well X1. The table specifically highlights the important parameters related to the IPR and VLP matching. The tubing head pressure remained constant at 590 psia for both the input and matched data. The tubing head temperature remained constant at 92.5 °F in both scenarios. The watercut is given as 0%, suggesting no presence of water in the oil for both the input and matched data.

The initial input for the liquid production rate was 675 STB/day. The pressure gauge was placed at a depth of 4,541 ft for both the input and matching data. The gauge pressure was measured at 1,967 psia for the input data. The initial reservoir pressure was measured at 2,016 psia, while the gas-oil ratio (GOR) was reported as 256 scf/STB.

Following the completion of the matching process, the liquid rate was marginally modified to 680 STB/day. The data analysis reveals a minor decline in reservoir pressure to 2,008 psia. The minor modifications in fluid flow rate and underground pressure between the initial input and the calibrated data likely indicate the refinement of the well model to better simulate the actual circumstances in the field during the DST. The match in GOR is highly significant, and implies that the model is accurately adjusted to the fluid characteristics of the reservoir fluid.

When comparing this to the literature, the matching procedure, in this case, seems to follow the usual pattern seen in DST and reservoir simulation research, where minor modifications are made to model parameters in order to align simulation findings with actual measured data. The small discrepancies between the input and matched data indicate a high level of precision in the initial model assumptions and the quality of the input data. According to Onwunalu and Durlofsky, a match of this level of accuracy suggests a reservoir system that is adequately characterized and a reliable

modeling approach.[35]

Fig. 5 illustrates the correlation between the IPR and VLP for a good test, likely Test 1. The IPR/VLP matching curve displays the calculated pressure values from the IPR model at various liquid rates (measured in STB/day). The curve follows a typical IPR pattern, starting at the initial reservoir pressure and dropping as the flow rate increases. The red squares on the curve reflect these computed pressure values. The Green Diamonds represent the measured pressure levels obtained from the well test (DST). These values are shown against the associated liquid rate. The green line remains horizontal, suggesting that the pressure recorded during the test did not show substantial variations with changes in the liquid rate. This suggests that the well test was done at a consistent bottom-hole pressure.

The liquid flow rate measured is 675 STB/day, with a gauge pressure of 2,017.2 psia. The liquid rate measured as "Test Calculated" is approximately 680.48 STB/day, with a gauge pressure calculated to be 2,008.13 psia. The "Test 1 % Difference" indicates negligible disparities between the measured and computed values, with the liquid rate difference being a mere 0.8102% and the pressure difference being 0.4499%. In the context of literature, the graph demonstrates a successful alignment in the calibration process of the well model. The close match between measured and calculated rates and pressures (< 1% difference) shows adequate characterization of the well and reasonable modeling of the reservoir flow phenomena. In literature, these matches are essential for verifying the predictive capability of reservoir simulation models and for establishing the model's reliability in making future performance predictions and reservoir management decisions.[36] The little variances fall below acceptable thresholds, indicating that the IPR and VLP models are accurately calibrated to the well's actual performance.

3.5 Scenarios for infill well placement optimization

Three scenarios were used to assess the impacts of well placement on additional oil recovery from a mature oilfield and how other selected factors confound the impact of infill well placement. The scenarios are outlined in section 3.3 and discussed in subsequent subsections.

3.5.1 Case 1: X1 production forecasting

Forecasting the production rates of Field X was conducted to assess the possible volumes that can be extracted. To achieve this, sophisticated dynamic reservoir modeling technologies, specifically Eclipse and Petrel RE, were utilized to predict production scenarios. The primary emphasis was placed on Well X1, the only fully constructed well within the reservoir, considering both its initial completion configuration and current perforation extent. Operational limitations were implemented to control the flow dynamics and simulate authentic production conditions. The defined limitations are as follows:

1. The production uptime of 95% ensures that the well was actively producing for most of its history.
2. The tubing head pressure (THP) must not exceed 100 psi to ensure the integrity of the well and effectively control

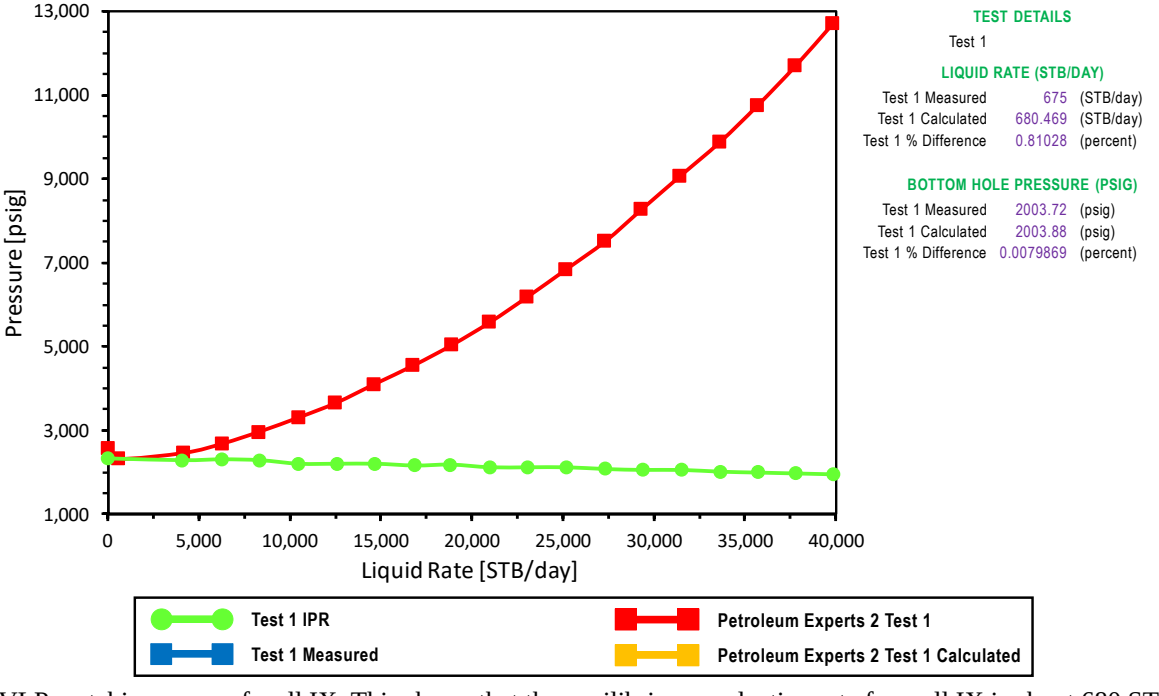

Fig. 5: IPR/VLP matching curve of well IX. This shows that the equilibrium production rate for well IX is about 680 STB/day with a bottomhole flow pressure of 2,003 psig. The maximum efficient rate can, therefore, be 675 STB/day.

Table 3: X1 well location and recovery from Field X.

X1 Location (I,J,K)	Perf interval avg. Perm. (mD)	Initial oil rate (STB/day)	Final oil rate (STB/day)	Final Watercut (%)	GOR (scf/STB)	Oil Cum. (MMSTB)	Recovery factor (R.F.)	Final pressure (psi)
41, 51, 1	623	3,856	187	76.8	242	1.75	0.022	1,788

production rates.

3. The maximum permissible watercut is 95%, which is the proportion of water produced relative to the total volume of fluids.
4. The establishment of a fixed minimum oil production rate of 100 RB/day is necessary to ensure economic sustainability.
5. The perforation intervals were accurately determined between 4,650 and 4,680 feet measured depth (MD), to focus on the most productive zones.

The parameters were carefully set up in the development strategy section of Petrel RE. Afterwards, the Eclipse simulator conducted a prediction run, providing a prognosis for a period of 10 years. Table 3 systematically organizes comprehensive data on the geographical arrangement of Well X1, the average permeability in the perforation period, and its associated recovery potential.

Table 3 provides information regarding Well X1 in Field X, including its geographical coordinates, production characteristics, and rates of recovery. This table presents the life cycle of well X1, including initial and final production rates, as well as economic limits for water cuts and reservoir pressure. These factors serve as important indicators for devising future production strategies and recovery methods. The good coordinates (I, J, K) are specified as 41, 51, 1 within the reservoir grid, indicating its position in the three-dimensional space of the grid model. With 623 mD permeability, the reservoir fluid will readily flow to the perforations. This is evident in the initial production rate of 3,856 STB/day, showing good productivity. Over time, the well experiences a substantial decrease in its production rate, reaching 187 STB/day, which is a common occurrence when the reservoir gradually becomes depleted. The final watercut of 76.8% suggests that most of the produced fluid is water, and the well is nearing its economic limit (which was initially set as 95%). The gas-oil ratio of 242 scf/STB is within the average range for numerous reservoirs and is considered moderate. The aggregate oil extracted from the well is documented as 1.75 MMSTB. The recovery factor, given as 0.022 or 2.2%, shows the fraction of the initial oil in place that has been successfully extracted. The ultimate reservoir pressure is measured at 1,788 psi, signifying a decrease in initial reservoir pressure and reservoir decline.

The production and pressure histories of well X1 in Field X are presented in Fig. 6. The plots include the history of gas production rate, oil production rate, cumulative oil production rate, watercut, and reservoir pressure trends. Based on projections for the years 2025-2034, Fig. 6 displays the outcomes of a three-dimensional dynamic model of the X1 well recovery rates. As the well ages, its production profile becomes more typical: oil rate decreases, watercut increases due to the presence and activity of the underlying aquifer, reservoir pressure drops slightly, and the GOR stays fairly constant. The well is approaching the end of its productive life, which means that water management will likely become an important concern. This knowledge is vital for reservoir management and future planning. Maintaining a consistent GOR over time is depicted in Fig. 6(a). Throughout the production period, there is little change in the amount of gas produced per barrel of oil. This is in part because the reservoir remained undersaturated for most of the well's history. In Fig. 6(b), the oil production rate and cumulative oil production are presented. With the well continuously producing oil, albeit declining, the cumulative oil production continuously increases. Reservoir pressure drops marginally over time, as seen in Fig. 6(c). This gradual decline is in part due to the strength of the underlying aquifer, which consistently replaces the voidage in the reservoir, leading to a much slower reservoir pressure decline. Fig. 6(d) represents the watercut percentage. It shows a steep rise at the beginning of the predicted period and then levels out at about 76.8%. This corroborates the inference on the strength of the aquifer, which slows reservoir pressure decline while resulting in a steeply increasing watercut.

Well, X1 was placed in a zone with moderate heterogeneity next to a shale streak, suggesting that it did not target the structurally higher sections, or "up-dip", of the reservoir, according to the 3D geological model. Early and rapidly increasing water production in this geological environment is supported by the 77% watercut, and a significant decrease in oil production rate over time. Uneven fluid flow and early water breakthrough, whether from an aquifer influx or injection, can result from the formed heterogeneities and nearby flow barriers, such as facies discontinuities in the production zones due to shale. Findings from the study suggest

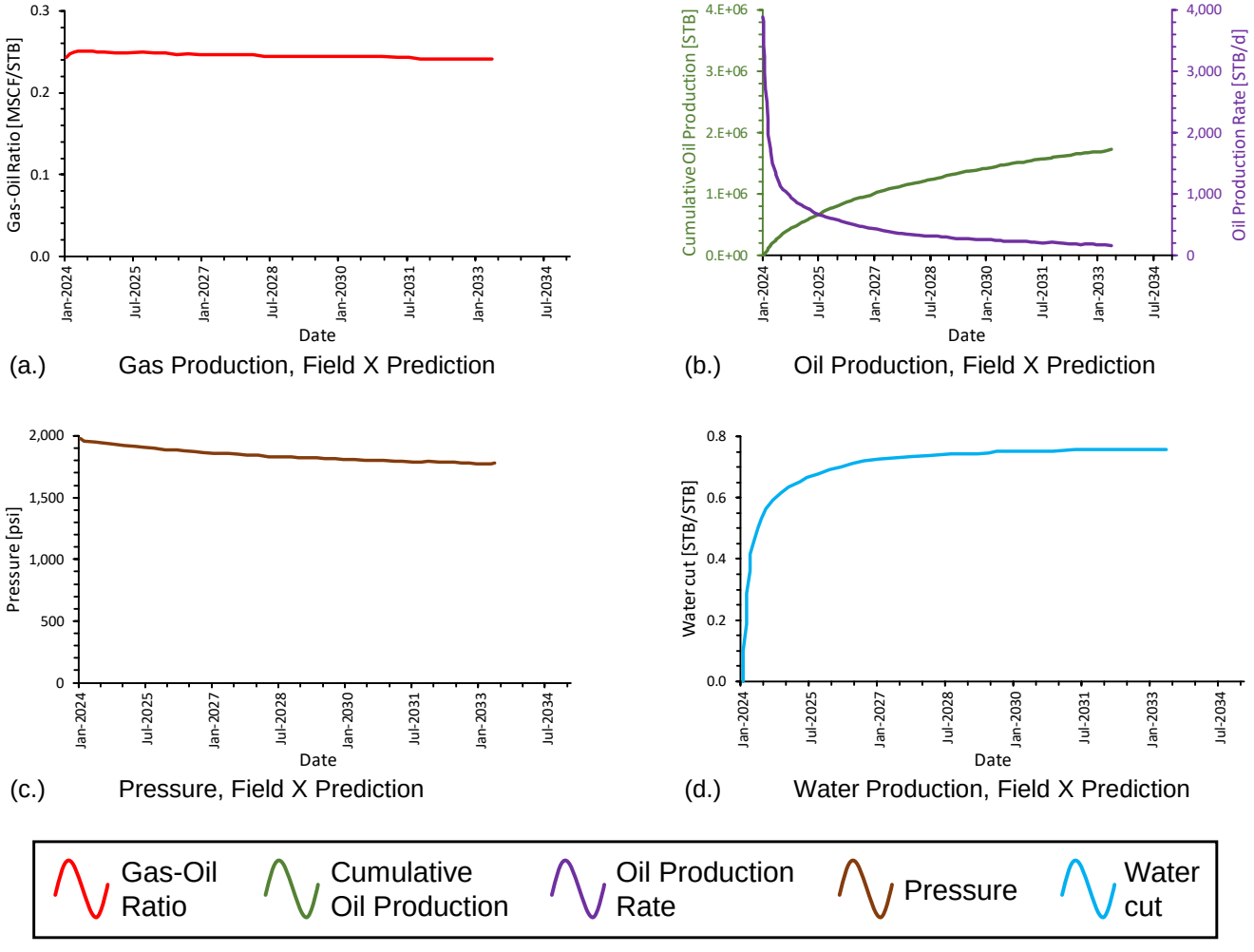

Fig. 6: X1 recovery rates from 3D dynamic simulation for well X1, where (a) well gas-oil ratio, (b) well oil production rates and well cumulative oil production, (c) well bottom-hole flowing pressure, and (d) well water cut.

that strategically placing infill wells, with considerations of the factors that lead to suboptimal performance of infill wells, can improve hydrocarbon recovery. This is because infill wells are drilled to reach the more productive zones of the reservoir for hydrocarbon extraction or to produce from areas with substantial remaining reserves in the reservoir despite continued production. Characteristics of such "sweet spots include high permeability, a large oil column height, low water saturation, little-to-no shale barriers, and high oil saturation.

A petrophysical analysis tool known as a net oil map can be used to visually depict the reservoir's sweet spots, which are locations with higher hydrocarbon saturations.[37] Critical in identifying the zones with the highest hydrocarbon potential, reservoir parameters such as thickness, porosity, water saturation, and permeability are integrated to build the map. Optimal well placement relies on these maps, which are crucial for reservoir characterization because they show changes in reservoir quality and pinpoint locations with a high production potential. The net oil map, which is depicted in Fig. S7, is based on the static reservoir model. The red circle represents the ideal area to drill infill wells. Infill drilling has the potential to greatly improve oil recovery with minimal water production in this area, which has an estimated oil column of about 12.5 feet.

3.5.2 Case 2: Infill-1X well production prediction

This study involved the strategic design of an infill well, Infill-1X, to tap into the reservoir's identified sweet spot, which has an oil column of 12.5 feet. While the general methodology of the Infill-1X simulation was comparable to that of the previous Well X1, there were some differences in the inputs used for the two, including the well site and the lift curves for the production system. Because they affect the well's deliverability, these lift curves, which show how well the system can pump fluids up from the reservoir - are crucial for production forecasts. Infill-1X was likewise subject to operational constraints to control the flow dynamics and mimic real-world production circumstances, similar to those that were applied to Well X1. In contrast to Well X1, the perforation interval for Infill-1X was defined as 4,626 to 4,640

Table 4: Infill-1X well location and recovery from X-field reservoir.

X1 Location (I,J,K)	Perf interval avg. Perm. (mD)	Initial oil rate (STB/day)	Final oil rate (STB/day)	Final watercut (%)	GOR (scf/STB)	Oil Cum. (MMSTB)	Recovery factor (R.F.)	Final pressure (psi)
48, 68, 1	1,120	2937	360	62	245	2.55	0.031	1,822

feet measured depth. Geological and petrophysical data were used to determine this depth range to maximize hydrocarbon recovery.

In order to gauge Infill-1X's prospective performance over the next decade, a production forecast covering that time period was prepared. Table 4 compiles the relevant data for this well, which includes measures like cumulative oil production, watercut, oil production rate, gas-oil ratio (GOR), and trends in reservoir pressure. Table 4 details the Infill-1X well, including its position, performance, and "final" reservoir pressure of Field X, which are crucial for planning and evaluation of infill drillingoperations for effective reservoir management. The well is located within the 3D reservoir model with the specified grid coordinates of 48, 68, and 1. At the hole interval, the average permeability is 1,120 mD, suggesting a very permeable zone that should allow for efficient fluid flow. The initial production rate was 2,937 STB/day, indicating good reservoir connectivity and well productivity. The GOR was 245 scf/STB, which is within the black oil range. Cumulative oil production from Infill-1X was estimated to be 2.55 MMSTB, representing about 3.1% of the initial hydrocarbon in place being recovered by Infill-1X over the ten years. Thanks to the strong underlying aquifer that consistently replaces voidage from Field X, the reservoir pressure declined gradually, from 2,106 to 1,822 psia. Again, the strength of the aquifer is confirmed by the higher watercut (62%) in the ten-year production history.

Production and pressure history of well Infill-X1 in Field X are presented in Fig. 7. The plots include the history of gas production rate, oil production rate, cumulative oil production rate, water-cut, and reservoir pressure trends. Based on projections for the years 2025 – 2034, Fig. 7 displays the outcomes of a 3D dynamic model of Infill-X1 well recovery rates. To produce an accurate prediction of Infill-1X's production while controlling for the modeling uncertainties, the simulation applies the same constraints and modeling methodologies as the current well but with modifications to account for the infill well's unique characteristics. Throughout the forecast period, there is little change in the amount of gas produced per barrel of oil, as shown in Fig. 7(a). This is in part because the reservoir remained undersaturated for most of the well's history. In Fig. 7(b), the oil production rate and cumulative oil production are presented. With the well continuously producing oil, albeit declining, the cumulative oil production continuously increases. This trend may suggest that the well initially has a high productivity, perhaps because of the high pressure, but subsequently it decreases as the reservoir pressure decreases and the well is stabilized.[11]

Reservoir pressure drops marginally over time, as seen in Fig. 7(c). This gradual decline is in part due to the strength of the underlying aquifer, which consistently replaces the voidage in the reservoir, leading to a much slower reservoir pressure decline. Fig. 7(d) represents the water-cut percentage. It shows a sharp rise at the beginning of the predicted period and then levels out at about 62%. This sharp increase, due to early water breakthroughs, results from the strength of the underlying aquifer. This almost instantaneously replaces the voidage in Field X, leading to a very low reservoir pressure decline. Another consequence of this strong underlying aquifer is that, with a slow reservoir pressure decline, the reservoir pressure mostly remains above the bubble-point pressure of the reservoir fluid, meaning that the GOR, and subsequently, gas production rate, will remain fairly constant. The "fairly constant" gas production rate due to the "fairly constant" GOR is illustrated in Fig. 7(a).

Fig. 7 provides data that is in agreement with typical production patterns found in undersaturated oil reservoirs with strong underlying aquifers. A rapidly increasing watercut can pose severe operational challenges for Field X. This is because the rapidly increasing produced water needs to be treated to meet global, regional, and local environmental standards before disposal. The slow reservoir pressure decline, which is due to the strong aquifer, means that Field X has good natural support, which could substantially improve its ultimate recovery.[38]

Infill-1X successfully intersected the reservoir at an up-dip site, which is recognized as a structurally higher and possibly more hydrocarbon-rich area, according to the spatial analysis of its well trajectory on the 3D reservoir model. In theory, the "fairly homogeneous" rock and fluid properties throughout Infill-1X's perforation interval in Field X should allow for a more predictable flow of fluids because the perforations of Infill-1X were located inside a zone of reasonable homogeneity. Nonetheless, fluid mobility can be affected, and

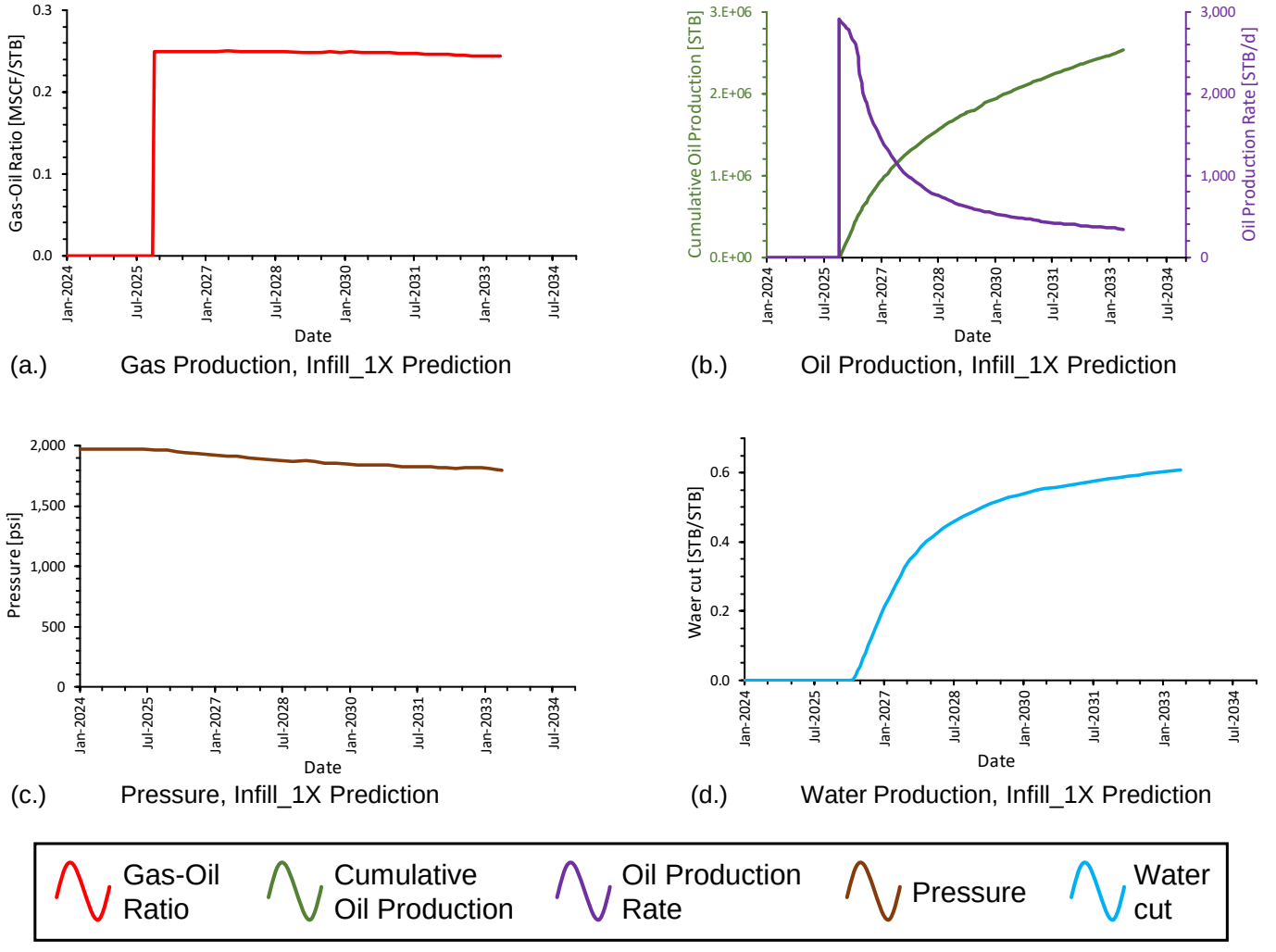

Fig. 7: Infill-1X recovery rates from 3D dynamic simulation, where (a) well gas-oil ratio, (b) well oil production rates and well cumulative oil production, (c) well bottom-hole flowing pressure, and (d) well water cut.

water production can eventually increase due to its closeness to the reservoir edge, a boundary that often indicates a change to a lower energy environment.[39]

As fluid dynamics on the flank push water towards the wellbore, the water drive mechanism explains the observed steady rise in water production after the breakthrough, culminating in a 62% watercut after ten years. Placing it in a homogeneous zone helps keep the production profile steady and predictable, according to Darcy's Law, whereas fluid flow in a heterogeneous zone might be unpredictable because of different permeabilities. An improvement in hydrocarbonextraction efficiency relative to Well X1 is seen in the reported recovery factor of 3.1% for Infill-1X. Because oil is less dense than water, it tends to gather at structural highs. By strategically placing the well, we may optimize oil recovery by targeting areas with higher hydrocarbon saturation and leveraging gravity forces. Drilling in a "homogeneous" zone also makes recovery calculations more reliable and helps to lower the uncertainty of output forecasts.

3.5.3 Case 3: Infill-2X well production prediction

Further evaluation of the reservoir flow dynamics of Field X was carried out using simulations of an additional infill well (Infill-2X) to identify the causes of early water breakthrough and potentials for improved hydrocarbon recovery. Theoretically, reservoir engineering and geological principles underpin the Infill-2X placement. To improve oil recovery and delay water breakthrough, it is recommended to select a perforation interval distant from the reservoir flank. This will facilitate exploiting areas of the reservoir with higher oil column thickness, less water encroachment from the aquifer and consequently, higher hydrocarbon recovery. Furthermore, the goal of increasing the infill well's recovery factor and economic efficiency is to maximize contact with oil-saturated sections of the reservoir, which is associated with targeting a net oil map thickness.

Distal to the reservoir flank, well Infill-2X was placed to potentially reduce water encroachment and exploit a portion of the reservoir with a 10.25-foot determined net oil map

Table 5: Infill-2X well location and recovery from Field X.

X1 Location (I,J,K)	Perf. interval avg. Perm. (mD)	Initial oil rate (STB/day)	Final oil rate (STB/day)	Final watercut (%)	GOR (scf/STB)	Oil Cum. (MMSTB)	Recovery factor (R.F.)	Final pressure (psi)
28, 56, 1	972	611	462	0.0005	250	1.95	0.024	1894

thickness. In the simulations, the Infill-2X well used the same operating conditions as the 1X and Infill-1X wells. The simulation and production forecast were for 10 years, similar to Infill-1X. Using similar operating conditions and production forecast duration was necessary to enable comparison and analysis for multiple wells and scenarios. For Infill-2X, the best hydrocarbon-bearing zone was targeted by carefully choosing a hole interval between 4,458 and 4,463 foot measured depth. The results of the simulations for Infill-2X and Field X at the end of 10 years of production are presented in Table 5.

In the 3D grid system of the reservoir model, the well is located at 28, 56, 1. The well's perforation zone has an average permeability of 972 mD, suggesting a relatively higher permeability that will further enhance the productivity of Infill-2X. The initial oil production rate of Infill-2X is 611 STB/day, which is substantially lower than Infill-1X. However, the decline in oil production rate was not as much as Infill-1X, with a final oil production rate of 462 STB/day. This suggests that Infill-2X had aquifer support, leading to a slight decline in the oil production rate. Despite this aquifer support, the watercut remained near-zero, about 0.0005%, suggesting a nearly exclusive oil production. This is an advantage of placing the infill well away from the oil-water contact of the aquifer: slide decline in oil production rate over a long period with little water production. Another factor that led to delayed water breakthrough in Infill-2X is the production rate of the well. With a higher production rate, the risk of water coming and gas cusping (if there is an overlaying gas cap) substantially increases, leading to an early fluid (water and gas, respectively) breakthrough and its attendant challenges. The results of Infill-2X show that the well placement was well managed, leading to consistent production and relatively higher oil cumulative production.

The GOR of Infill-2X and Infill-2X remained at about 250 scf/STB. This is due to the high water influx from the aquifer (called strong aquifer support) and the consequent pressure maintenance. The reservoir pressure remained higher than the bubble-point pressure of the reservoir fluid. The cumulative oil production of Infill-2X for the 10 years was 1.95 MMSTB, which represents an oil recovery factor of 2.4% or 0.024. Despite the relatively low recovery factor from Infill-2X, the slight drop in reservoir pressure (final pressure of 1,894 psia compared to initial reservoir pressure of 2,016 psia) is indicative of the strong aquifer support and potential for a long productive life of Field X.

Based on the data in Table 5, it appears that Infill-2X was well-positioned to achieve high oil recovery rates with low water production. This was probably due to careful, good design that avoided water-bearing zones and targeted the reservoir's sweet spots. For future reservoir management strategy planning and to assess the drilling operation's success, the statistics reflecting the well's performance over the anticipated period are crucial.

Production and pressure histories of Infill-2X in Field X are presented in Fig. 8. The plots include the history of gas production rate, oil production rate, cumulative oil production rate, watercut, and reservoir pressure trends. Based on projections for the years 2025–2034, Fig. 8 displays the outcomes of a 3D dynamic model of Infill-2X recovery rates. The gas production rate of Infill-2X was essentially constant throughout the 10-year production history, as shown in Fig. 8(a). This is in part because the reservoir remained undersaturated for most of the well's history. The slight reservoir pressure decline, which led to the reservoir pressure remaining above the bubble-point of the reservoir fluid, was facilitated by the strong support from the underlying aquifer.

In Fig. 8(b), the oil production rate and cumulative oil production are presented. The oil production rate remained fairly constant for 10 years. With the relatively lower production rate compared to Infill-1X, and the apposite well placement, Infill-2X did not encounter water breakthrough throughout the 10 years. This fairly constant oil production rate is corroborated by the near-linear cumulative oil production over the 10 years. There was a steady but slight decline in reservoir pressure, as shown in Fig. 8(c). This is in part because the well was placed away from the aquifer, though still benefitting from the strong aquifer support.

In Fig. 8(d), the watercut percentage is presented. The watercut reached 0.0005%, showing that there was essentially

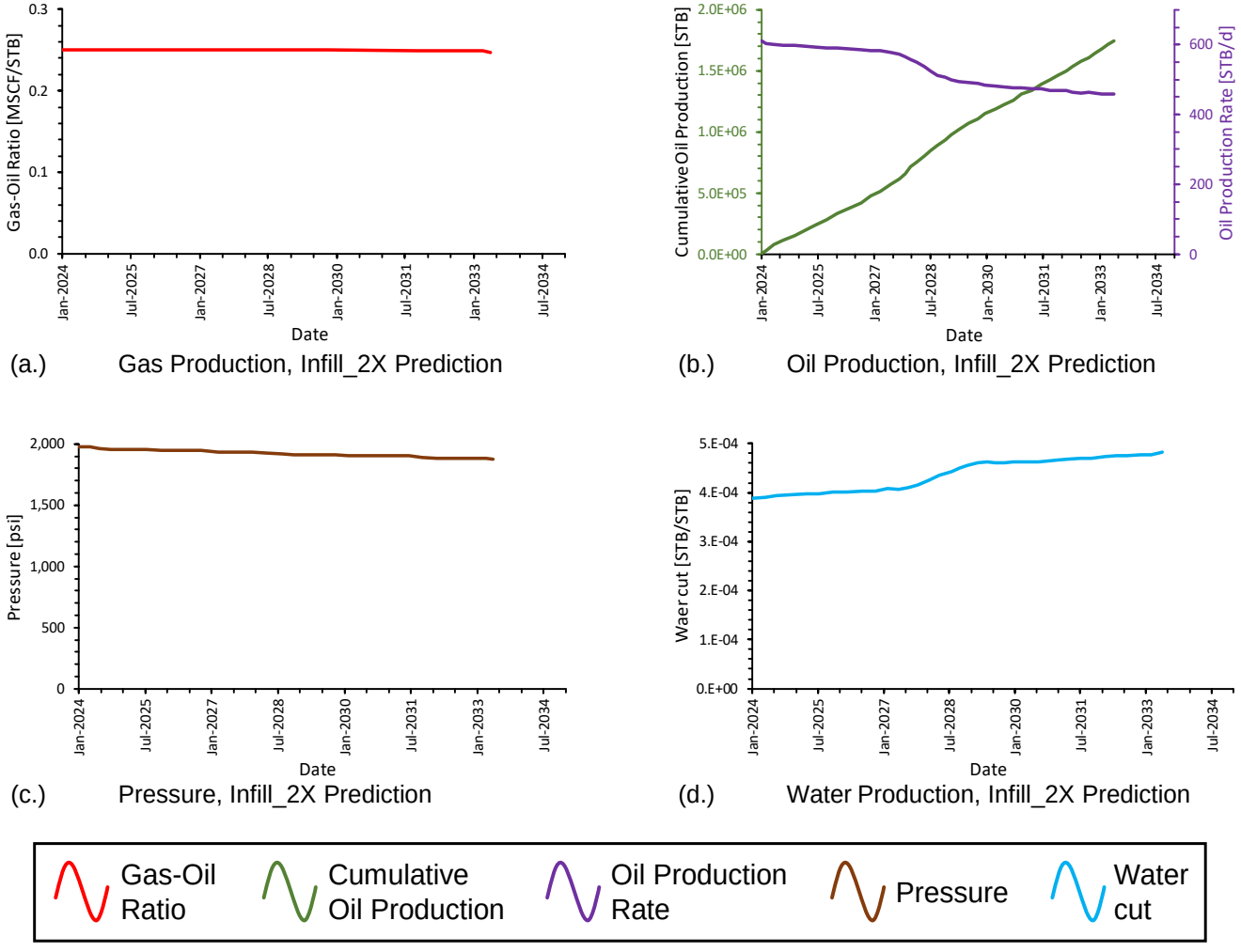

Fig. 8: Infill-2X recovery rates from 3D dynamic simulation, where (a) well gas-oil ratio, (b) well oil production rates and well cumulative oil production, (c) well bottom-hole flowing pressure, and (d) well water cut.

no water production from Infill-2X throughout the 10 years. This is corroborated by the near-linear decline in the oil production rate. This strongly highlights the importance of optimizing infill well placement in a reservoir of interest, leading to higher oil production, lower watercut and consequently, a higher hydrocarbon recovery. With proper infill well placement, the economic life of the reservoir is extended. In this reservoir, despite placing Infill-2X away from the aquifer, the strength of the aquifer was felt by Infill-2X, as shown in the fluid production rates and the slight decline in reservoir pressure.

3.6 Prediction results comparison

The importance of well placement within an underground hydrocarbon reservoir for optimizing recovery efficiency is shown by the comparison of these three cases presented in Table 6. The ranking of average permeability at the perforatio intervals in the wells is: Case 2 > Case 3 > Case 1. Despite this ranking, the initial oil production rates are ranked as Case 1 > Case 2 > Case 3. The production declines of these three scenarios were also substantially different over the 10 years: Case 1 had a production decline of 95.15%; Case 2 had 87.74%; Case 3 had 24.39%. The ranking of the water-cuts is: Case 1 > Case 2 > Case 3. The ranking for cumulative oil production from the scenarios is Case 2 > Case 3 > Case 1. Interestingly, despite having a substantially lower initial production rate compared to Case 1, Case 3 has a higher "final" oil production rate and higher cumulative oil production over the 10 years.

This strongly highlights the importance of proper well placement in facilitating improved production and a longer economic life for the reservoir of interest. The best approach, therefore, is to strike a compromise between controlled production rate and high permeability.[40] To keep a steady production profile with low watercut and GOR, it is essential to use a moderate production rate to reduce the chances of quick pressure depletion and excessive water production. In maintaining hydrocarbon production rates and extending the well's economic life, the Case 3 scenario demonstrates a balanced approach for harmonizing contributing factors while

Table 6: Recovery comparison by well location from Field X.

Cases	Perf interval avg. Perm. (mD)	Initial oil rate (STB/day)	Final oil rate (STB/day)	Final watercut (%)	GOR (scf/STB)	Oil Cum. (MMSTB)	Recovery factor (R.F)	Final pressure (psi)
1	623	3,856	187	76.8	242	1.75	0.022	1,788
2	1,120	2,937	360	62	245	2.55	0.031	1,822
3	972	611	462	0.0005	250	1.95	0.024	1,894

improving fluid recovery.

Recovery metrics for various well instances in Field X are compared in Table 6. Case 1 has the lowest permeability (623 mD) and the highest initial oil rate (3,856 STB/day). Due to the large final watercut of 76.8%, the oil rate decreases dramatically to 187 STB/day. The last pressure was 1,788 psi, and the recovery factor was 0.022, the lowest. In contrast to Case 1, which had an initial oil rate of 2,937 STB/day and a permeability of 1,120 mD, Case 2 had the opposite problem. Despite this, it keeps the watercut at a lower 62% and the ultimate oil rate at a superior 360 STB/day. There is a small increase to 1,822 psi in the final pressure relative to Case 1, and the recovery factor improves to 0.031. In Case 3, the watercut is a mere 0.0005%, and the oil rate goes from 611 STB/day, the lowest, to 462 STB/day, the greatest. It reaches a maximum final pressure of 1,894 psi and a recovery factor of 0.024 with a modest permeability of 972 mD.

Based on the comparison of these situations, it can be observed that higher initial permeability is associated with better sustainability of production rates and less watercuts over time, but it does not necessarily mean higher initial production rates. In Case 3, we see that a moderate and controlled production strategy yields the best final oil production rate and the lowest watercut, even if the initial production rate was the lowest. According to reservoir engineering principles like Darcy's law, higher permeability helps to obtain improved sustained production rates. The principles of fluid flow in porous media, which include a controlled production rate to minimize excessive water production owing to coning or encroachment, are also consistent with the significant drop in the final watercut in Case 3.

These findings, when compared to previous research, highlight the need for well-management plans that take both short-term production potential and long-term recovery objectives into account. According to the literature, the best way to recover is to maintain reservoir pressure and prevent premature water breakthrough by balancing reservoir features, well placement, and regulated production techniques.[41] The modeling and forecasting methodologies used in this study are viable because the recovery factors and watercuts given are within realistic ranges observed in similar field case studies. In the section that follows, we will use the Darcy equation to further validate these conclusions, taking into account differences in permeability as a measure of reservoir heterogeneity. Using Darcy's equation, we can measure how permeability variations affect the fluid flow and check if the production trends we have observed match up with how fluids should behave theoretically in reservoirs made of different rocks. The strategy's applicability and the alignment of production forecast with basic reservoir engineering principles depend on this validation.

3.7 Validation of results

In order to validate the simulation findings against the Darcy flow equation, several fundamental assumptions are made to ensure consistency with the principles of Darcy's law. The assumptions are: (i) the reservoir fluid has a fairly constant density (or incompressible), indicating that the flow does not experience substantial variations in volume with changes in pressure; (ii) the movement of fluid through the rock in the reservoir is caused by a difference in pressure, as explained by Darcy's law. This law indicates that the rate of flow is directly proportional to the difference in pressure supplied to the porous material.[42] It is assumed that the viscosity of the fluid remains constant during the flow process, which makes calculations simpler, as viscosity is a variable in Darcy's equation. Permeability is often considered to be constant over time at a specific place. However, it is recognized that it can vary in different areas of the reservoir due to geological differences.

The validation process relies on the data obtained from reservoir fluid characterization (PVT analysis), as well as information about reservoir and fluid-rock characteristics, and the unique details of the well configuration. The validation process incorporates constant parameters such as the viscosity of the fluid, the oil formation volume factor (Bo), the thickness of the reservoir, the radius of the wellbore, and the overall radius of the reservoir. The only factor to consider is permeability, which takes into account the fact that the infill

Table 7: Input parameters for well placement dynamic simulation validation.

Avg. reservoir thickness (ft)	Viscosity (cP)	FVF (RB/STB)	Wellbore radius (ft)	Reservoir radius (ft)	Drawdown (psi)	Well 1X Perm. (mD)	Well infill-1X Perm. (mD)	Well infill-2X Perm. (mD)
320	7.02	1.132	0.354	7,475.82	50	623	1,120	972
Validation: Estimated flow rate q (STB/day)						892.12	1,603.81	1,391.88

wells are located in areas with considerable heterogeneity. Thus, adhering to these assumptions, Darcy's law will be applied to estimate the flow rates by Eq. 4:[43]

$$Q = \frac{kA \cdot \Delta P}{\mu L} \quad (4)$$

where the flow rate (Q) is a function of permeability (k), the pressure differential (ΔP), the cross-sectional area through which the flow occurs (A), and the fluid's viscosity (μ), and L is the length over which the pressure differential occurs.

The validation method entails the comparison between the 3D simulation results and the flow rates derived using Darcy's equation, utilizing the aforementioned input parameters. Table 7 shows the validation data and the related flow rate results obtained from Darcy's equation. This will serve as a rigorous assessment of the theoretical model.

Table 7 presents the input parameters utilized to validate the dynamic simulation for well placement and the computed flow rates for three wells in Field X, employing Darcy's Law. The permeability values for each well and the estimated flow rates are as follows:

The 1X Perm has a permeability of 623 mD and is expected to have a flow rate of 892.12 STB/day. The permeability of Well Infill-1X is 1,120 mD, with an estimated flow rate of 1,603.81 STB/day. The Infill-2X Perm has a permeability of 972 mD and is expected to have a flow rate of 1,391.88 STB/day.

When comparing these validated results to the earlier results obtained from Cases 1, 2, and 3, Case 1 (Well 1X) exhibited an initial high rate of oil production that rapidly declined to a lower ultimate rate accompanied by a substantial increase in water proportion. The validated projected flow rate of 892.12 STB/day is lower than the initial oil rate obtained from the simulation, but it is closer to the ultimate oil rate. Case 2 (Well Infill-1X) exhibited a lower decline in oil production rate and a reduced watercut over time, compared to Case 1. This may be attributed to the relatively higher permeability of Case 2 (1,120 mD compared to 623 mD for Case 1).

Using Darcy's equation, Case 2 has an oil production rate of 1,603.81 STB/day, meaning that it can produce more than the current conditions. Besides the reservoir heterogeneities not captured in Darcy's equation, another factor contributing to this discrepancy is the strength of the aquifer, which contributes to a higher water production rate with a declining oil production rate. Case 3 (Well Infill-2X) exhibited the lowest initial production rate, although it achieved the highest ultimate production rate and an extraordinarily low final watercut. The confirmed flow rate of 1,391.88 STB/day corresponds closely to the elevated final production rate recorded throughout the simulation.

The flow rates predicted from the validation of Darcy's law typically support the patterns found in the dynamic simulation results: wells with a higher permeability tend to maintain higher production rates. Nevertheless, the simulated flow rates may be reduced as a result of unconsidered elements in the Darcy equation validation, including reservoir heterogeneity, wellbore conditions, completion efficiency, and other contributing factors in reservoir performance, like the strength of a nearby aquifer. The findings highlight the relationship between the characteristics of the reservoir and the effectiveness of production, confirming the validity of the simulation method and emphasizing the significance of strategic well positioning and permeability in optimizing the oil recovery from a reservoir of interest.

3.8 Summary of findings

In this study, comprehensive 3D simulations analysis, and validation using Darcy's law were conducted to maximize hydrocarbon recovery from mature oilfields using strategic infill well placement. Based on the results obtained, the reservoir permeability is a key factor in determining the optimal locations for infill wells. The study compared three scenarios: an existing well (Case 1), and two infill wells (Cases 2 and 3) placed in different locations. The key findings include:

1. Higher permeability zones generally maintain better production rates over time.
2. Strategic well placement away from water-bearing zones (Case 3) resulted in minimal water production and sustained oil rates.
3. Moderate, controlled production strategies (Case 3)

yielded the best final oil production rates and lowest water cut.
4. Initial high production rates do not necessarily indicate a long-term good performance.
5. The strength of the underlying aquifer significantly impacts the production dynamics and water breakthrough timing.

The study emphasizes that well planning with integrated reservoir modeling, supported by dynamic simulations and geophysical data, can extend the productive life of mature fields and enhance the overall hydrocarbon recovery. Additionally, the results were validated by Darcy's flow equations, reinforcing the significance of permeability in predicting well performance and recovery potential.

4. Conclusion

The importance of strategically placing infill wells to maximize reservoir recovery is highlighted in this study. The distribution of remaining hydrocarbon saturation and the dynamic reservoir features that affect fluid flow are analyzed in detail. It has been brought to light that reservoir permeability is an important factor that dictates where infill wells should be placed. The study's thorough 3D dynamic simulation analysis supported this viewpoint and led to the following important conclusions. The results, obtained from the 3D dynamic simulations and verified using Darcy's law, validate the crucial significance of strategic well positioning and the function of reservoir permeability in maximizing oil recovery in a reservoir of interest, such as Field X, which was used in this study. The effectiveness of targeted drilling in high permeability zones and the avoidance of water-bearing flanks is demonstrated by Infill-1X and Infill-2X. This leads to higher recovery rates and reduced watercut. This study effectively demonstrates a correlation between the theoretical characteristics of fluid flow in porous media and practical reservoir development tactics. The simulation results, which are more conservative than the validation of Darcy's law, indicate that the actual performance of the well may surpass the projected forecasts. This provides a positive outlook for the economic feasibility of Field X. By integrating simulation data with theoretical modeling using Darcy's equation, and a comprehensive strategy is provided for future initiatives regarding well placement and production. This technology allows for the identification of ideal drilling locations that achieve a balance between the potential for immediate production and the long-term goals of maximizing reservoir recovery. This ensures sustainable development and management of the reservoir.

Conflict of Interest

There is no conflict of interest.

Supporting Information

Applicable.

References

[1] D. Koroteev, Z. Tekic, Artificial intelligence in oil and gas upstream: Trends, challenges, and scenarios for the future, *Energy and AI*, 2021, **3**, 100041, doi: 10.1016/j.egyai.2020.100041.
[2] S. I. Aanonsen, A. L. Eide, L. Holden, J. O. Aasen, Optimizing reservoir performance under uncertainty with application to well location, SPE Annual Technical Conference and Exhibition, October 22-25, Dallas, Texas, 1995, doi: 10.2118/30710-ms.
[3] V. Artus, L. J. Durlofsky, J. Onwunalu, K. Aziz, Optimization of nonconventional wells under uncertainty using statistical proxies, *Computational Geosciences*, 2006, **10**, 389-404, doi: 10.1007/s10596-006-9031-9.
[4] O. Badru, C. S. Kabir, Well placement optimization in field development, SPE Annual Technical Conference and Exhibition, October 5-8, Denver, Colorado, 2003, doi: 10.2118/84191-ms.
[5] W. Bangerth, H. Klie, M. F. Wheeler, P. L. Stoffa, M. K. Sen, On optimization algorithms for the reservoir oil well placement problem, *Computational Geosciences*, 2006, **10**, 303-319, doi: 10.1007/s10596-006-9025-7.
[6] V. Bukshtynov, O. Volkov, L. J. Durlofsky, K. Aziz, Comprehensive framework for gradient-based optimization in closed-loop reservoir management, *Computational Geosciences*, 2015, **19**, 877-897, doi: 10.1007/s10596-015-9496-5.
[7] Z. Bouzarkouna, D. Y. Ding, A. Auger, Well placement optimization with the covariance matrix adaptation evolution strategy and meta-models, *Computational Geosciences*, 2012, **16**, 75-92, doi: 10.1007/s10596-011-9254-2.
[8] Z. Bouzarkouna, D. Y. Ding, A. Auger, Well placement optimization under uncertainty with CMA-ES using the neighborhood, ECMOR XIII-13th European Conference on the Mathematics of Oil Recovery, 2012, cp-307, doi: 10.3997/2214-4609.20143200.
[9] Y. Cheng, D. A. McVay, W. J. Lee, A practical approach for optimization of infill well placement in tight gas reservoirs, *Journal of Natural Gas Science and Engineering*, 2009, **1**, 165-176, doi: 10.1016/j.jngse.2009.10.004.
[10] J. Hutahaean, V. Demyanov, M. Christie, Reservoir development optimization under uncertainty for infill well placement in brownfield redevelopment, *Journal of Petroleum Science and Engineering*, 2019, **175**, 444-464, doi: 10.1016/j.petrol.2018.12.043.
[11] M. G. Chu, B. Min, S. Kwon, G. Park, S. Kim, N. X. Huy, Determination of an infill well placement using a data-driven multi-modal convolutional neural network, *Journal of Petroleum Science and Engineering*, 2020, **195**, 106805, doi: 10.1016/j.petrol.2019.106805.
[12] A. Malallah, A. Alashwak, I. S. Nashawi, Infill well placement optimization in two-dimensional heterogeneous reservoirs under waterflooding using upscaling wavelet

transform, *Journal of Petroleum Science and Engineering*, 2021, **201**, 108439, doi: 10.1016/j.petrol.2021.108439.
[13] E. S. Gladchenko, A. E. Gubanova, D. M. Orlov, D. A. Koroteev, Kriging-boosted CR modeling for prompt infill drilling optimization, *Petroleum*, 2024, **10**, 39-48, doi: 10.1016/j.petlm.2023.09.003.
[14] A. A. Emerick, E. Silva, B. Messer, L. F. Almeida, D. Szwarcman, M. A. C. Pacheco, M. M. B. R. Vellasco, Well placement optimization using a genetic algorithm with nonlinear constraints, SPE Reservoir Simulation Symposium, February 2-4, The Woodlands, Texas, 2009, doi: 10.2118/118808-ms.
[15] S. Ding, H. Jiang, J. Li, G. Tang, Optimization of well placement by combination of a modified particle swarm optimization algorithm and quality map method, *Computational Geosciences*, 2014, **18**, 747-762, doi: 10.1007/s10596-014-9422-2.
[16] P. S. da Cruz, R. N. Horne, C. V. Deutsch, The quality map: a tool for reservoir uncertainty quantification and decision making, *SPE Reservoir Evaluation & Engineering*, 2004, **7**, 6-14, doi: 10.2118/87642-pa.
[17] G. Alusta, E. Mackay, J. A. Fennema, K. A. Armih, Decision making tool to assist in choosing between polymer flooding and infill well drilling: case study, SPE Asia Pacific Enhanced Oil Recovery Conference, July 2-4, Kuala Lumpur, Malaysia, 2013, doi: 10.2118/165276-ms.
[18] A. Cottini-Loureiro, M. Araujo, Optimized well location by combination of multiple realization approach and quality map methods, SPE Annual Technical Conference and Exhibition, October 9-12, Dallas, Texas, 2005, doi: 10.2118/95413-ms.
[19] Akhil Datta-Gupta and Michael J. King, Streamline simulation: theory and practice, Richardson, Texas: Society of Petroleum Engineers, 2007, 15-30, ISBN: 978-1-61399-939-4.
[20] N. Y. Guerra, R. Narayanasamy, Well location selection from multiple realizations of a geomodel using productivity potential maps-A heuristic technique, International Oil Conference and Exhibition in Mexico, August 31-September 2, Cancun, Mexico, 2006, doi: 10.2118/102903-ms.
[21] B. Güyagüler, R. N. Horne, Uncertainty assessment of well placement optimization, SPE Annual Technical Conference and Exhibition, September 30-October 3, New Orleans, Louisiana, 2001, doi: 10.2118/71625-ms.
[22] F. E. Jansen, M. G. Kelkar, Upscaling of reservoir properties using wavelets, SPE India Oil and Gas Conference and Exhibition, February 17-19, New Delhi, India, 1998, doi: 10.2118/39495-ms.
[23] S. Kang, A. Datta-Gupta, W. J. Lee, Impact of natural fractures in drainage volume calculations and optimal well placement in tight gas reservoirs, *Journal of Petroleum Science and Engineering*, 2013, **109**, 206-216, doi: 10.1016/j.petrol.2013.08.024.
[24] A. Kharghoria, M. Cakici, R. Narayanasamy, R. Kalita, S. Sinha, Y. Jalali, Productivity-based method for selection of reservoir drilling target and steering strategy, SPE/IADC Middle East Drilling Technology Conference and Exhibition, October 20-22, Abu Dhabi, United Arab Emirates, 2003, doi: 10.2118/85341-ms.
[25] J. Kikani, M. He, Multi-resolution analysis of long-term pressure transient data using wavelet methods, SPE Annual Technical Conference and Exhibition, September 27-30, New Orleans, Louisiana, 1998, doi: 10.2118/48966-ms.
[26] N. Liu, Y. Jalali, Closing the loop between reservoir modeling and well placement and positioning, Intelligent Energy Conference and Exhibition, April 11-13, Amsterdam, The Netherlands, 2006, doi: 10.2118/98198-ms.
[27] T. Lee, D. Jeong, S. Jang, J. Kim, C. Mo, H. Jeong, J. Choe, Infill well placement optimization using integrated asset modeling technique, SPE/IATMI Asia Pacific Oil & Gas Conference and Exhibition, October 29-31, 2019, Bali, Indonesia, 2020, doi: 10.2118/196299-ms.
[28] G. M. Shook, K. M. Mitchell, A robust measure of heterogeneity for ranking earth models: The F-PHI curve and dynamic lorenz coefficient, SPE Annual Technical Conference and Exhibition, October 4-7, New Orleans, Louisiana, 2009, doi: 10.2118/124625-ms.
[29] Tarek H. Ahmed, Fundamentals of hydrocarbon phase behavior, in equations of state and PVT analysis: applications for improved reservoir modeling, Cambridge, MA: Gulf Professional Publishing, Elsevier, 2016, 1-69, ISBN: 978-0-12-801570-4.
[30] M. J. Zandvliet, M. Handels, G. M. van Essen, D. R. Brouwer, J. D. Jansen, Adjoint-based well-placement optimization under production constraints, *SPE Journal*, 2008, **13**, 392-399, doi: 10.2118/105797-pa.
[31] S. Taware, H. Y. Park, A. Datta-Gupta, S. Bhattacharya, A. K. Tomar, M. Kumar, H. S. Rao, Well placement optimization in a mature carbonate waterflood using streamline-based quality maps, SPE Oil and Gas India Conference and Exhibition, March 28-30, Mumbai, India, 2012, doi: 10.2118/155055-ms.
[32] B. Yeten, L. J. Durlofsky, K. Aziz, Optimization of nonconventional well type, location, and trajectory, *SPE Journal*, 2003, **8**, 200-210, doi: 10.2118/86880-pa.
[33] S. Vlemmix, G. Joosten, Brouwer, J. Jansen, Adjoint-based well trajectory optimization in a thin oil rim, SPE Europec featured at EAGE Conference and Exhibition, June 8-11, Amsterdam, The Netherlands, 2009, doi: 10.2118/121891-ms.
[34] L. Nakajima, D. J. Schiozer, Horizontal well placement optimization using quality map definition canadian, International Petroleum Conference, Calgary, Alberta, Petroleum Society of Canada, 2003, doi: 10.2118/2003-053.
[35] J. E. Onwunalu, L. J. Durlofsky, Application of a particle swarm optimization algorithm for determining optimum well location and type, *Computational Geosciences*, 2010, **14**, 183-198, doi: 10.1007/s10596-009-9142-1.
[36] U. Ozdogan, A. Sahni, B. Yeten, B. Guyaguler, W. H. Chen, Efficient assessment and optimization of a deepwater asset development using fixed pattern approach, SPE Annual Technical Conference and Exhibition, October 9-12, Dallas, Texas, 2005, doi: 10.2118/95792-ms.
[37] M. N. Panda, C. Mosher, A. K. Chopra, Application of wavelet transforms to reservoir data analysis and scaling, SPE Annual Technical Conference and Exhibition, October 6-9, Denver, Colorado, SPE, 1996, doi: 10.2118/36516-ms.

[38] M. R. Rasaei, M. Sahimi, Upscaling of the permeability by multiscale wavelet transformations and simulation of multiphase flows in heterogeneous porous media, *Computational Geosciences*, 2009, **13**, 187-214, doi: 10.1007/s10596-008-9111-0.
[39] A. Centilmen, T. Ertekin, A. S. Grader, Applications of neural networks in multiwell field development, SPE Annual Technical Conference and Exhibition, October 3-6, Houston, Texas, 1999, doi: 10.2118/56433-ms.
[40] A. Salmachi, M. Sayyafzadeh, M. Haghighi, Infill well placement optimization in coal bed methane reservoirs using genetic algorithm, *Fuel*, 2013, **111**, 248-258, doi: 10.1016/j.fuel.2013.04.022.
[41] E. Annan Boah, O. Kwami Senyo Kondo, A. Aidoo Borsah, E. T. Brantson, Critical evaluation of infill well placement and optimization of well spacing using the particle swarm algorithm, *Journal of Petroleum Exploration and Production Technology*, 2019, **9**, 3113-3133, doi: 10.1007/s13202-019-0710-1.
[42] A. O. Arinkoola, H. M. Onuh, D. O. Ogbe, Quantifying uncertainty in infill well placement using numerical simulation and experimental design: case study, *Journal of Petroleum Exploration and Production Technology*, 2016, **6**, 201-215, doi: 10.1007/s13202-015-0180-z.
[43] T. Ahmed, Fundamentals of rock properties, Reservoir Engineering Handbook, Amsterdam: Elsevier, 2010, 189-287, ISBN: 978-1-85617-803-7.50012-2.